Carbohydrate Polymer Technologies and Applications 13 (2026) 101069

Contents lists available at ScienceDirect

Carbohydrate Polymer Technologies and Applications

journal homepage: www.sciencedirect.com/journal/carbohydrate-polymer-technologies-and-applications

Tuning the biological scaffolds' performance by the combination of two antioxidant and antimicrobial chitosan derivatives

C. Muñoz-Núñez [a,b,c], A. Barco-Martín [a], K. Deshpande [d], D.S. Schmidt [d], L. González-García [d,e], S. Trujillo [d,*], A. Muñoz-Bonilla [a,b,*], M. Fernández-García [a,b,*]

[a] Instituto de Ciencia y Tecnología de Polímeros (ICTP-CSIC), C/Juan de la Cierva 3 Madrid 28006, Spain
[b] Interdisciplinary Platform for Sustainable Plastics towards a Circular Economy-Spanish National Research Council (SusPlast-CSIC), Madrid, Spain
[c] Facultad de Ciencias Químicas, Universidad Complutense de Madrid, Avenida Complutense s/n, Ciudad Universitaria, Madrid 28040, Spain
[d] INM-Leibniz Institute for New Materials, Campus D2 2, Saarbrücken 66123, Germany
[e] Saarland University, Department of Materials Science and Engineering, Campus D2 2, Saarbrücken 66123, Germany

ARTICLE INFO

Keywords:
Scaffolds
Chitosan
Modification
Antimicrobial
Antioxidant
Immunology

ABSTRACT

In this study novel polymeric materials based on chitosan (CS) were synthesized by chemically modifying CS with two bioactive moieties: eugenol and a compound containing a thiazolium group. These modifications aimed to impart antioxidant and antimicrobial properties to the matrix. Additionally, the scaffolds were reinforced with chitin nanowhiskers (Nw) to improve their mechanical strength and stability. Porous three-dimensional scaffolds were fabricated via the freeze-drying process, resulting in highly interconnected pore networks suitable for cell infiltration and nutrient transport. Biological characterization revealed that the incorporation of the two bioactive groups significantly enhanced the antioxidant activity and antimicrobial efficacy against both Gram-positive and Gram-negative bacteria to the scaffolds. Mechanical testing demonstrated that the Nw reinforcement increased scaffold stiffness and resilience without compromising porosity. In vitro biological assays using fibroblasts showed favorable cytocompatibility and promoted sustained cell proliferation over three weeks. Fluorescence microscopy confirmed fibroblast adhesion and morphological adaptation within the scaffold architecture. Additionally, the scaffolds were evaluated for their immunomodulatory effects using macrophage cultures, revealing a balanced immune response with reduced proinflammatory signaling, which is critical for successful integration and reduced fibrosis in vivo. These results indicate that those are promising candidates for tissue engineering and regenerative medicine applications.

1. Introduction

Chitin (Ch) is the second most abundant polysaccharide in nature after cellulose, found in the exoskeletons of crustaceans, insects or crabs (Terkula Iber et al., 2022). This polysaccharide is composed of repeating units of N-acetyl-D-glucosamine linked through β-(1→4) bonds, which confer a highly crystalline and rigid structure (Moussian, 2019). This biopolymer can be modified and processed in various ways to produce functional materials, depending on the chemical or mechanical treatment applied (Phongying et al., 2007; Sriupayo et al., 2005). One of its most relevant derivatives is chitin nanowhiskers (Bai et al., 2022; Muñoz-Nuñez et al., 2022; Muñoz-Núñez et al., 2024) (Nw), nanoscale structures obtained by acid hydrolysis of the polymer, which exhibit higher crystallinity and enhanced mechanical properties. These nanomaterials are often used as reinforcing agents in polymer matrices to develop hybrid systems with improved physicochemical characteristics (Chi-Yan Li et al., 2016; D. Li et al., 2020; Paillet & Dufresne, 2001).

Furthermore, chitin can be easily transformed into chitosan (CS) through partial or complete deacetylation of its N-acetyl groups (Muñoz-Bonilla et al., 2019). This chemical transformation not only modifies its structure but also changes its physicochemical properties, due to the presence of free amino groups (Korpayev & Ahmed, 2021), which gives it a positive charge in acidic environments (W. Wang et al., 2020). CS is the only naturally cationic polysaccharide (Korpayev, Toprak et al., 2020), which allows the biopolymer to easily interact with negatively charged biological components (such as bacterial surfaces or certain proteins) and also enables its chemical modification to enhance or introduce new functionalities (Q. Chen et al., 2022), such as

* Corresponding authors.
E-mail addresses: Sara.TrujilloMunoz@leibniz-inm.de (S. Trujillo), sbonilla@ictp.csic.es (A. Muñoz-Bonilla), martafg@ictp.csic.es (M. Fernández-García).

https://doi.org/10.1016/j.carpta.2025.101069

Available online 16 December 2025

antioxidant (J. Liu et al., 2017) or antimicrobial (Cui et al., 2022) activity. CS is known for its biocompatibility (Martău et al., 2019), biodegradability (Matica et al., 2017), low cost (Mohan et al., 2022) non toxicity (Kamarul et al., 2014) and simply processed (Ciarlantini et al., 2025; Gholap et al., 2024; Homayoni et al., 2009; Mallakpour et al., 2021; Peers et al., 2020; van den Broek et al., 2015; Yang et al., 2010). All these properties situate this polymer as an attractive candidate for many applications (Abourehab et al., 2022; Muñoz-Nuñez et al., 2025) such as food packaging (H. Wang et al., 2018), drug delivery (Bernkop-Schnürch & Dünnhaupt, 2012), wound healing (Ding et al., 2022; W. Liu et al., 2023) or tissue engineering (Croisier & Jérôme, 2013), among other .

From a chemical perspective, to provide CS with additional functional properties (Jiménez-Gómez & Cecilia, 2020), chemical modification through the incorporation of bioactive molecules could be proposed. In this work, the introduction of two compounds with known biological activities is explored: eugenol (EU) and thiazole molecules. EU is a natural phenolic compound present in several essential oils (Marchese et al., 2017) (such clove, cinnamon, turmeric…) and it is known for its strong antioxidant activity, although its antiseptic, anti-inflammatory, and antimicrobial properties are also well studied in the literature (Almeida Alima et al., 2024; Jung et al., 2006; Khadim et al., 2024; Kowalewska & Majewska-Smolarek, 2023; Sauperl et al., 2021; Valencia-Sullca et al., 2024). This molecule contains a hydroxyl group and an allylic double bond, which makes it reactive and suitable for covalent bonding to polymers like CS. On the other hand, thiazole molecules exhibit a great spectrum of biological properties (Muñoz-Nuñez et al., 2023; Tejero et al., 2015; Zhao et al., 2015), including antimicrobial (Mohamed et al., 2022), antiviral (Ibrahim et al., 2022), and anticancer activities (Dawood et al., 2013). Taking advantage of their ability to be quaternized, the thiazolium ring increases the positive charge of the molecule (Fabiano et al., 2020; Martins et al., 2014; Shagdarova et al., 2019), enhancing its interaction with bacterial membranes, destabilizing the membrane and causing the bacteria to die. When those molecules were covalently linked to CS, the antimicrobial action was intensified without compromising the natural structure or biocompatibility of the polymer.

We hypothesized that incorporating bioactive derivatives and reinforced nanoparticles into CS scaffolds would enhance their functional properties without compromising their biocompatibility and physicochemical and mechanical properties. This approach is expected to overcome the existing limitations of these materials in tissue engineering, focusing on tissue regeneration or implantable biomaterials by giving intrinsic and potent antimicrobial and antioxidant characteristics and improved structural stability. To prove the hypothesis, CS scaffolds were prepared incorporating mixtures of CS derivatives based on EU and thiazolium molecules (10 wt %) and chitin nanowhiskers (1 wt %). These were selected because they present antioxidant and antimicrobial characteristics and strengthening capacity, respectively. This multifunctional approach aims to generate structurally robust and biologically active scaffolds with only a small percentage of active CS derivatives.

2. Materials and methods

Chitosan (from shrimp shells, with a deacetylation degree exceeding 75 %) with a molecular weight of 357 ± 10 kDa, a degree of deacetylation determined by NMR of 77 %, and chitin (Ch, also from shrimp shells) were procured from Merck. From this biopolymer, chitin nanowhiskers (Nw) with a length average of 123 ± 16 nm were subsequently produced using an acid hydrolysis method (Muñoz-Núñez et al., 2024). Additional reagents, including glycerol (gly, 99 %), 6-hydroxy-2,5,7,8-tetramethylchroman-2-carboxylic acid (Trolox, 97 %), and 2,2-diphenyl-1-picrylhydrazyl (DPPH), were also acquired from Merck. Genipin (Gp) and lysozyme (sourced from egg white) were supplied by Fisher Scientific.

Table 1
Composition of chitosan scaffolds (wt. %).

Sample	CS (%)	CS-EU (%)	CS-MTBAQ (%)	Nw (%)	Gly (%)
CS	85	-	-	-	15
CS-EU0-MT10	75	-	10	-	15
CS-EU2.5-MT7.5	75	2.5	7.5	-	15
CS-EU5-MT5	75	5	5	-	15
CS-EU7.5-MT2.5	75	7.5	2.5	-	15
CS-EU10-MT0	75	10	-	-	15
CS-Nw	84	-	-	1	15
CS-EU0-MT10-Nw	74	-	10	1	15
CS-EU2.5-MT7.5-Nw	74	2.5	7.5	1	15
CS-EU5-MT5-Nw	74	5	5	1	15
CS-EU7.5-MT2.5-Nw	74	7.5	2.5	1	15
CS-EU10-MT0-Nw	74	10	-	1	15

The chemically modified chitosan derivatives, namely CS-MTBAQ (Muñoz-Nuñez et al., 2023) and CS-EU (Muñoz-Núñez et al., 2025) were synthesized according to published procedures previously reported by our group and present modification degree of 0.68 % and 50 %, respectively. All organic solvents used in this work were of analytical grade. Glacial acetic acid, concentrated hydrochloric acid (HCl, 37 %), and methanol (MeOH) were supplied by Scharlau.

For biological assays, sodium chloride (NaCl, cell culture grade, BioXtra) and phosphate-buffered saline (PBS, pH 7.4) were purchased from Merck. Mueller-Hinton broth, used for bacterial growth, was acquired from Becton, Dickinson and Company. Microplates (96-well) were obtained from ThermoFisher Scientific. Columbia blood agar plates enriched with 5 % defibrinated sheep blood were sourced from Fisher. The microbial strains used in this study included *Escherichia coli* (*E. coli,* ATCC 25,922)*, Staphylococcus aureus* (*S. aureus* ATCC 29,213)*, Enterococcus faecalis* (*E. faecalis*, ATCC 29,212) and *Pseudomonas aeruginosa (P. aeruginosa*, ATCC 27,853), all provided by Oxoid™.

In the context of cell culture, Dulbecco's Phosphate Buffered Saline (DPBS), Dulbecco's Modified Eagle Medium (DMEM), and a Penicillin-Streptomycin (P/S) antibiotic mixture were purchased from Gibco. The 3-(4,5-dimethylthiazol-2-yl)-2,5-diphenyltetrazolium bromide (MTT reagent) and Triton X-100 was obtained from Sigma-Aldrich. Heat-inactivated fetal bovine serum (FBS, 65 °C for 30 min) was provided by PAN Biotech. AlamarBlue™ Cell Viability Reagent came from Invitrogen.

Additional reagents and kits included sodium dodecyl sulfate (SDS, ≥99.5 %), bovine serum albumin (BSA), Paraformaldehyde solution (PFA, 4 %), DAPI (4′,6-diamidino-2-phenylindole, dihydrochloride), CoraLite-488-labeled phalloidin (in sterile water, Proteintech), the Micro BCA™ Protein Assay Kit, and the LIVE/DEAD™ Viability/Cytotoxicity Kit for mammalian cells, all obtained from Thermo Fisher Scientific. The Mouse interleukin-6 (IL-6) DuoSet ELISA Kit was obtained from R&D Systems, and QuantiBlue™ reagent and murine macrophages (J774 Dual™) were purchased from InvivoGen. Normal human dermal fibroblasts (NHDF-Ad) supplied by Lonza.

2.1. Chitosan scaffold preparation

Chitosan scaffolds were fabricated using a freeze-drying method to obtain a highly porous structure suitable for cellular interaction. CS (1 % w/v) was dissolved in a 1 % (v/v) acetic acid solution under constant stirring until a homogeneous solution was achieved. The modified CS derivatives, CS-EU and CS- MTBAQ, were incorporated into the solution at predefined ratios (0–10, 2.5–7.5, 5–5, 7.5–2.5, and 10–0), ensuring complete dispersion. Additionally, for enhanced mechanical properties, 1 % (wt. %) of Nw were added to selected formulations. To improve flexibility and stability, 15 % (w/v) glycerol was incorporated into all compositions, adjusting the relative proportions (Table 1). Glycerol also

contributes to regulating the crystallization process during freeze-drying, preventing the formation of excessively sharp ice crystals that could compromise the porous microstructure of the scaffolds.

After homogenization, the solutions were stirred for 24 h to ensure proper mixing. The resulting mixtures were then cast into 96-well polystyrene plates and subjected to a controlled freezing process. Once frozen, the samples were lyophilized to remove the solvent, yielding a porous scaffold structure.

Following lyophilization, the scaffolds were crosslinked by immersion in a 0.025 % genipin solution in PBS and incubated at 37 °C for 24 h. This process produced a color change from white to dark green, indicating successful crosslinking. To remove excess genipin, the scaffolds were washed twice with ethanol and subsequently rinsed with distilled water. Finally, the scaffolds were frozen again and subjected to a second lyophilization step before storage under same conditions until further characterization and testing.

The incorporation of different CS-EU/CS-MTBAQ ratios allowed for the evaluation of their combined effect on the scaffold properties, while the inclusion of Nw provided additional structural reinforcement

2.2. Microstructural characterization

The morphological analysis of the scaffolds was conducted using scanning electron microscopy (SEM) to evaluate both the internal structure and surface characteristics. To prepare the samples, the scaffolds were fractured using liquid nitrogen to obtain clean cross-sections, ensuring an accurate visualization of the internal porosity and structural organization.

The morphology was analyzed using a SNE Alpha SEM with an acceleration voltage of 20 kV. Prior to visualization, the samples were coated with a layer of Au/Pd (80/20) to enhance electron conductivity and improve imaging quality. The SEM analysis was performed under high vacuum conditions at varying magnifications to assess pore size and distribution. ImageJ software was used to process and analyze the obtained micrographs, allowing for quantitative evaluation of structural parameters such as pore diameter and interconnectivity.

2.3. Interconnectivity

A liquid displacement method was used to evaluate the interconnectivity of the scaffolds. The scaffolds were immersed in an inert organic solvent, ethanol, at a controlled volume of 0.5 mL (density 0.789 g/cm^3) and incubated at 20 °C for 30 min (Ciarlantini et al., 2024). After this time, excess liquid was carefully removed, and the samples were weighed. By comparing the weight before and after immersion, the volume of displaced liquid was determined, providing an estimation of the internal porosity and degree of interconnectivity of the scaffolds (Eq. (1)).

$$Interconnectivity\ (\%) = \left(\frac{W_{final} - W_{initial}}{\rho_{EtOH} \times V_{initial}}\right) \times 100 \quad (1)$$

2.4. Absorption capacity

The ability of the scaffolds to absorb liquid was evaluated using Dulbecco's Modified Eagle Medium (DMEM), a standard medium in cell culture studies. Scaffolds were immersed in 1 mL of DMEM at 37 °C for 24 h to allow for absorption (Drozdova et al., 2023). The initial weight of each scaffold was recorded before immersion, and the final weight was measured after removing any excess medium. The absorption capacity was determined by calculating the weight difference, which represents the amount of DMEM absorbed (Eq.2).

$$Absorption\ (\%) = \left(\frac{W_{final} - W_{initial}}{W_{initial}}\right) \times 100 \quad (2)$$

2.5. Rheological properties

Before testing, all samples were immersed in PBS for 24 h at room temperature (22–23 °C) to ensure complete hydration. After equilibrating the scaffolds, the analysis was performed using a MCR702e rheometer equipped with an 8 mm stainless-steel parallel plate geometry (Anton Paar, Austria). Oscillatory amplitude sweep tests ranging from 0.01 % to 100 % strain at a constant frequency of 10 rad/s were performed to determine the linear viscoelastic (LVE) region and evaluate the strength of the network. Quantification of the mechanical stability was done via the values of the crossover of storage modulus (G') and the loss modulus (G''), describing elastically stored or dissipated energy, respectively. Each scaffold formulation underwent ten replicate measurements under identical conditions. The resulting data was processed to calculate mean values with corresponding standard deviations, ensuring statistically reliable characterization of the viscoelastic properties.

2.6. Protein adsorption

Quantification of the protein adsorption on the scaffolds was assessed using the MicroBCA™ Protein Assay Kit. The scaffolds were then placed in a 96-well plate and to evaluate the amount of protein retained on the scaffold surface, samples were initially incubated with 100 µL of BSA solution at a concentration of 200 µg/mL for 2 h. After incubation, the scaffolds were washed twice with PBS to remove any non-adsorbed proteins and transferred to a new well plate.

Then, the scaffolds were immersed in 200 µL of 1 % SDS solution, shake for 30 min to desorb the proteins. Subsequently, 150 µL of the resulting solution of SDS with the proteins desorbed were transferred to a 96-well plate with 150 µL of the MicroBCA working reagent and incubated at 37 °C for 2 h in the dark. Absorbance was measured at 562 nm using a microplate reader (TECAN Spark), and protein content was determined by comparing the results to a standard calibration curve of BSA concentrations ranging from 0 to 200 µg/mL prepared in PBS. All experiments were performed in triplicates.

2.7. Antioxidant activity

For the assay, a stock solution of DPPH was prepared by dissolving 15 mg of DPPH in 250 mL of methanol. Each scaffold was immersed in 1 mL of this solution and incubated in the dark. The decrease in absorbance at 517 nm was measured hourly during the first 8 h and other two samples at 16 h and 24 h, to determine the scavenging activity over time. All samples were tested in triplicate.

$$DPPH\ scavenging\ (\%) = \left(\frac{Absorbance_{control} - Absorbance_{sample}}{Absorbance_{control}}\right) \times 100 \quad (3)$$

2.8. Antimicrobial properties

The antimicrobial activity of the scaffolds was evaluated following the ASTM E2149–20 standard method (*ASTM E2149–20, Standard Test Method for Determining the Antimicrobial Activity of Antimicrobial Agents Under Dynamic Contact Conditions; ASTM International.* www.astm.org), which assesses the ability of materials to reduce bacterial viability in dynamic contact conditions. The antibacterial performance was tested against both Gram-positive and Gram-negative bacteria, including *S. aureus, E. faecalis, E. coli* and *P. aeruginosa* bacteria.

Scaffolds were immersed in a bacterial suspension (1 mL) with an initial concentration of 10^6 CFU/mL of each bacteria in PBS and incubated under continuous agitation at 100 rpm at 37 °C to ensure uniform contact between the material and the microorganisms for 24 h (Chiloeches et al., 2022). After this time, serial dilutions were done and plated onto agar plates for counting and incubated again at 37 °C for 24

h. All experiments were performed in triplicate to ensure reproducibility.

2.9. Cytotoxicity and proliferation studies

The scaffolds were first sterilized by exposure to UV radiation for 30 min on each side. After sterilization, they were hydrated with a FBS solution for 30 min at 37 °C(Miranda et al., 2016). The cells were cultured in fibroblast basal medium (FBM), supplemented with 10 % FBS, FGM-2 SingleQuots (fibroblast growth supplement medium containing insulin, human basic-fibroblast growth factor (hFGF-B), and gentamicin sulphate amphotericin (GA-1000)), and 1 % penicillin-streptomycin) at 37 °C in a 5 % CO_2 atmosphere. Medium was exchanged every other day and fibroblasts were passaged upon 70 % confluency.

Once sterilized and treated with FBS, the scaffolds were placed in untreated 96-well plates. Around 10,000 cells were seeded onto each scaffold. After an incubation of 24 h, the scaffolds with the adhered fibroblasts were moved to a new untreated plate to guarantee that only cells attached to the scaffolds were analyzed, removing any cells on the sides of the wells.

Cell proliferation was evaluated using the Alamar Blue assay at 1, 2, 3, 7, 14, and 21 days. Alamar Blue reagent (10 % v/v) was added to each well containing the samples and cells and, were incubated at 37 °C for 2 h. Then, the medium was transferred to black 96-well plates, and fluorescence was measured (Ex/Em 570/600 nm) using the microplate reader.

Controls included scaffolds of each type without cells (negative control) and scaffolds with fibroblasts cultured in a standard 96-well plate (positive control) to ensure proper cell adhesion.

2.10. Cell staining

Cells were stained to assess their morphology at different times. Cells were fixed with 4 % PFA for 1 h at 4 °C. After fixation, the scaffolds were washed twice with PBS to remove any residual fixative. Subsequently, the samples were permeabilized using 0.1 % Triton X-100 in PBS for 15 min at room temperature. Then, the scaffolds were washed twice with PBS. The samples were covered with the DAPI/phalloidin staining solution and incubated for 30 min at room temperature in complete darkness. After that, they were gently washed twice with PBS.

2.11. Fibroblast morphology analysis

Fibroblast adhesion, distribution and proliferation on the scaffolds were evaluated through SEM using an SNE Alpha equipment. A dehydration protocol was implemented, progressing through an ethanol gradient series to gradually replace aqueous media without inducing structural collapse. When fully dried, the scaffolds were coated via sputter deposition (Au/Pd alloy, 80:20 ratio).

2.12. Macrophage cell culture

Macrophages were maintained in complete DMEM growth medium under culture conditions of 37 °C and 5 % CO_2. Scaffolds were sterilized by UV for 30 min per surface. Around 10,000 cells were seeded per well in 96-well plates and allowed to adhere for 24 h. Different scaffold formulations were then added to the wells with fresh medium, along with control groups: cell-free scaffolds (negative control) and LPS-stimulated macrophages (15 ng/mL, positive control). Following 24 h coculture, 150 µL supernatant aliquots were collected. Three independent replicates were analyzed per experimental group.

2.13. QuantiBlue assay

The activation of J774-Dual cells following scaffold exposure was monitored by measuring the expression of a secreted embryonic alkaline phosphatase (SEAP). J774-Dual cells are genetically modified to express SEAP under activation of NF-kB transcription factor. SEAP detection was carried out via QuantiBlue assay. 180 µL of QuantiBlue detection reagent were added to 20 µL of conditioned medium from the macrophage-scaffold cultures, negative controls and positive controls (0.1 µg/mL). Then, they were incubated for 30 min at 37 °C in dark conditions. Absorbance spectra (620–655 nm) were acquired using the microplate reader. Each experimental group was analyzed in triplicate.

2.14. Enzyme-linked immunosorbent assay (ELISA) for IL-6 quantification

IL-6 secretion was evaluated using a sandwich ELISA. A 96-well plate was initially coated with capture antibody (50 µL/well) and incubated overnight at room temperature in darkness. After three wash cycles with PBS containing 0.05 % Tween-20, non-specific binding sites were blocked with 300 µL/well of Reagent Diluent for 1 h. After this time, for antigen binding, the experimental supernatants prepared before (100 µL/well) were then incubated for 2 h with gentle agitation. Following another wash, the Detection Antibody (50 µL/well) was added and incubated for 2 h. After this time, the wells were washed again and the streptavidin-HRP conjugate (100 µL/well) added for 20 min. The wells were newly washed three times, and the substrate solution (100 µL/well) was added and let react for 20 min in darkness. The colorimetric reaction was stopped by adding stop solution (50 µL/well) and absorbance was immediately measured at 450 nm with 540 nm reference wavelength correction using a microplate reader. All conditions were analyzed in triplicate. Final cytokine concentrations were determined using a standard curve prepared from recombinant mouse IL-6 protein (pg/mL).

2.15. Live/Dead assay

Macrophage viability was evaluated after 24 h of scaffold exposure using the LIVE/DEAD™ Viability/Cytotoxicity Kit. The prepared staining solution was added directly to the cells, and the 96-well plate was incubated for 15 min at 37 °C, protected from light. After incubation, fluorescence images were acquired using a Keyence BZ-X810 All-in-one fluorescence microscope. A minimum of 10 images per sample were captured across multiple fields to ensure a representative analysis.

$$Viability(\%) = \frac{n^{\circ} live\ cells}{total\ cells} \times 100 \quad (4)$$

2.16. In vitro biodegradation

Enzymatic degradation assay was performed using lysozyme. Each scaffold was then immersed in 1 mL of a lysozyme solution (13 mg/L in PBS) and incubated at 37 °C with 60 rpm of agitation (Han et al., 2012). The degradation medium was refreshed every three days with a freshly prepared lysozyme solution in PBS. Samples, tested in triplicate, were collected weekly for 63 days to evaluate the degradation process by measuring the dry weight loss over time. The initial weight of each scaffold (w_0) was recorded before starting the experiment. Samples were taken once per week for 9 weeks. At each specific time, the medium was removed, the scaffolds were frozen, lyophilized, and then weighed again (w_1). The degradation rate was calculated using Eq. (5).

$$Weight\ lost\ (\%) = \left(\frac{W_0 - W_1}{W_0}\right) \times 100 \quad (5)$$

The potential cytotoxicity of soluble products generated during scaffold degradation was evaluated using a complementary viability assay with NHDF-Ad cells. Degradation media were collected and tested from the enzymatic degradation assay at 7, 28, and 63 days, to represent the early, intermediate and advanced stages of scaffold decomposition.

Table 2
Pore diameter of all prepared scaffolds and flow stress determined by the crossover of G' and G'', the yield stress and the flow transition index (FTI).

Sample	Pore diameter (μm)	Flow stress (Pa)	Yield stress (Pa)	FTI
CS	16.6 ± 6.9^{a}	53 ± 13	13 ± 3	4
CS-EU0-MT10	32.9 ± 16.5^{b}	73 ± 23	12 ± 4	6
CS-EU2.5-MT7.5	26.4 ± 8.4^{c}	87 ± 5	11 ± 4	8
CS-EU5-MT5	24.7 ± 9.9^{cd}	106 ± 27	13 ± 3	8
CS-EU7.5-MT2.5	$22.8 \pm 9.^{de}$	111 ± 28	11 ± 2	10
CS-EU10-MT0	21.7 ± 9.0^{ef}	103 ± 9	11 ± 2	9
CS-Nw	17.9 ± 8.3^{a}	42 ± 8	9 ± 5	5
CS-EU0-MT10-Nw	26.3 ± 10.9^{c}	79 ± 31	12 ± 5	7
CS-EU2.5-MT7.5-Nw	25.9 ± 11.6^{c}	95 ± 28	11 ± 4	9
CS-EU5-MT5-Nw	25.1 ± 7.7^{cd}	78 ± 9	11 ± 1	7
CS-EU7.5-MT2.5-Nw	24.4 ± 7.3^{cde}	118 ± 6	12 ± 2	10
CS-EU10-MT0-Nw	19.0 ± 7.4^{af}	101 ± 29	12 ± 2	8

Values having the same letter are not significantly different for Tukey test ($P \leq 0.05$).

2.17. Statistical analysis

Statistical comparisons among groups in the interconnectivity, fluid uptake, and cytotoxicity tests were achieved using one-way ANOVA. Tukey's test was used to identify specific differences between conditions. Statistical significance was established at $P \leq 0.05$. For all other experimental measurements, appropriate statistical treatment was also applied. In each case, data were obtained from at least three independent replicates per condition.

3. Results and discussion

3.1. Microstructural characterization

The morphological and mechanical properties of the scaffolds with different compositions were evaluated. All scaffolds exhibited a highly porous and interconnected architecture. Pore size characteristic of each scaffold formulation was determined by analyzing SEM images with ImageJ software, and the results are presented in Table 2.

The observed dimensions of the pores ranged from 16.6 μm to 32.9 μm. According to the literature (Karakeçili et al., 2022; Sharma et al., 2016), this range is suitable for promoting nutrient diffusion, oxygen transport throughout the scaffold, and the removal of waste products. In principle, these conditions would support cell growth, migration, and proliferation by providing an increased surface area for cell attachment and a structural network that supports 3D tissues formation (Abbasi et al., 2020; Hing et al., 2005).

All scaffolds exhibited a similar porous structure, however, differences in pore size were observed depending on the chemical composition of the CS derivative used (CS-EU or CS-MTBAQ). Although the differences are not statistically significant in every case, the results show that as the concentration of CS-MTBAQ increases (and CS-EU decreases), the pore size also increases. Previous studies (Gaweł et al., 2023; Kanimozhi et al., 2016; Medeiros Borsagli et al., 2018; D. Wang et al., 2015) have related the pore size to the polar nature of the CS derivatives, suggesting that their interaction with water can influence the pore structure during the lyophilization process. In this context, CS-EU, which contains more hydrophobic chains, would form a more compact system with reduced interaction with the solvent, resulting in smaller pores after freeze-drying.

Likewise, pore interconnectivity is another key parameter of the scaffolds for tissue engineering. Greater pore interconnectivity and number of pores provide more space for the cells' adaptation, migration into the scaffolds, and nutrient production (Korpayev, Kaygusuz et al., 2020). Moreover, a high degree of interconnectivity enhances the diffusion of nutrients and oxygen, and with the micropores, facilitates efficient transport and exchange of metabolic substances (Jiankang et al., 2007). The interconnectivity is shown in Fig. 1a.

The results indicate an interconnectivity of approximately 80 % for all compositions, which is suitable for supporting cellular infiltration in tissue engineering applications (Griffon et al., 2006; Kim et al., 2012).

In addition to pore structure, the ability of the scaffolds to absorb and retain the cell culture medium is crucial for creating a favorable environment for their growth. To evaluate this property, the absorption capacity of scaffolds was tested (Fig. 1b) using DMEM as a model fluid (M. Dash et al., 2011; Florczyk et al., 2013; Huang et al., 2019). No significant differences were observed in DMEM absorption capacity among the diverse scaffold compositions (Borges-Vilches et al., 2023). This could be explained by the fact that all scaffolds shared a common base of CS and Gly, with only 10 % of the composition altered by different modified CS. The absorption in scaffolds based on CS largely depends on pore structure, the proportion of CS, and the presence of the plasticizer, the dominant matrix governs the overall retention properties. If the chemical modifications do not alter surface chemistry or scaffold morphology, their influence on absorption remains limited. This suggests that the variations in pore size are minimal and do not affect the ability of the scaffolds to absorb the medium used. Therefore, all compositions can be considered suitable for supporting cell viability and proliferation.

The mechanical properties of the scaffolds were analyzed via oscillatory amplitude sweeps, and the storage (G') and loss (G'') moduli as a function of strain deformation are displayed in Figs. 1c (without Nw) and d (with Nw). All tested scaffolds show solid-like behavior, indicated by G' > G'' within the linear viscoelastic (LVE) region (G' independent of the applied strain). At the crossover value of G' and G'', the so-called flow point (see Table 2), the material transitions from solid-like to liquid-like behavior. Young's modulus (E) for each scaffold (see Table S1 in the Supporting Information) was calculated using G' values at the LVE region and the assuming a Poisson's ratio (ν) of 0.5 as follows:

$$E = 2G^{'(1+\nu)} \tag{6}$$

For scaffolds without added Nw, the addition of EU slightly increased the flow stress from 53 Pa (EU0-MT10) to 103 Pa (EU10-MT0). This can be attributed to the specific molecular structure and interactions of eugenol within the polymer matrix (Zeng et al., 2023). When adding Nws, the flow stress increased for the formulation without EU (79 Pa). Up to an EU content of 7.5 wt. %, the Nws enhance the flow stress compared to non-filled scaffolds, which we attribute to a reinforcement effect of the fillers (Petrova et al., 2020). This reinforcement effect seems to reach its limit at the highest concentration of EU, where the Nws do not show a significant improvement in the flow stress (101 Pa). At this EU concentration, the Nws hinder the interactions between the EU and the polymer matrix, reducing the overall mechanical stability. Surprisingly, this reinforcement effect has no significant impact on *E* values. All of them vary in the range 1.2–2.0 kPa (see Table S1), which is considered soft and adequate for fibroblast growth. In addition, the yield stress, which is the value of the shear stress at the limit of the LVE region, was also determined and the ratio between the flow stress and yield stress, viz. the flow transition index, was also estimated. The closer this ratio is to one, the greater the tendency of the sample to undergo brittle fracture (D. R. Dash et al., 2024; Mezger, 2020; Zhou et al., 2022). Therefore, all the studied scaffolds present a ductile nature.

3.2. Antioxidant properties

The evaluation of antioxidant properties in biomaterials has gained relevance in tissue engineering, especially in applications where oxidative stress could compromise cellular function and tissue regeneration (Fadilah et al., 2023; Gao et al., 2021). In this study, the

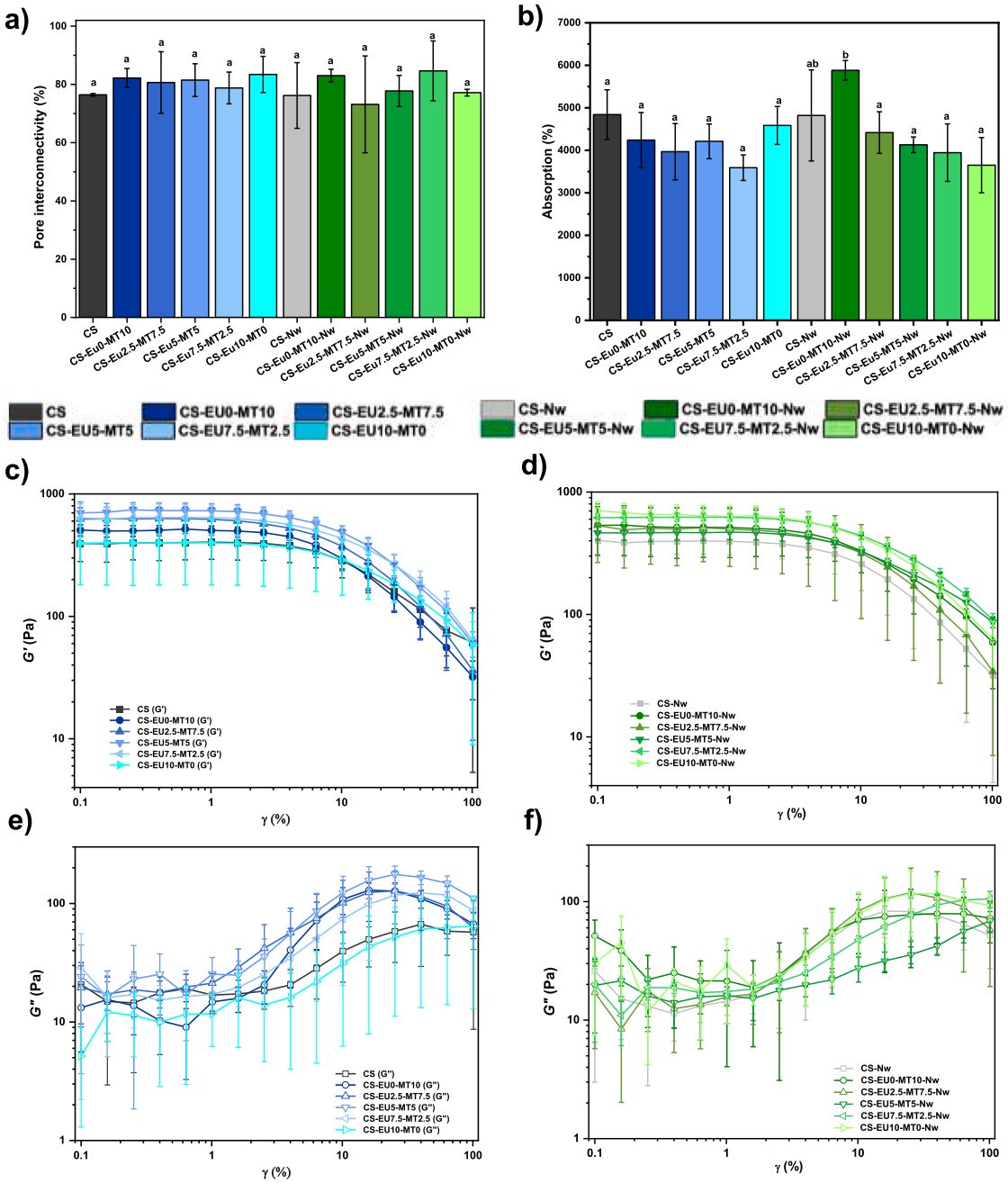

Fig. 1. Properties of scaffolds with varying compositions of CS-EU and CS-MTBAQ. (a) Percentage of pore interconnectivity, $n = 3$; (b) cell culture medium uptake $n = 3$ (%); Oscillatory amplitude sweeps of (c, e) scaffolds without Nw, $n = 10$ and (d, f) scaffolds with Nw, $n = 10$. Filled symbols indicate G' and open symbols G''. Solid lines are a guide to the eye.

antioxidant activity of scaffolds with different compositions was tested using the DPPH radical scavenging method, which enables the estimation of the material's capacity to neutralize free radicals.

Scaffolds containing different proportions of CS-EU and CS-MTBAQ were analyzed to investigate how the chemical composition influences the antioxidant behavior. This aspect is relevant due to the good properties of eugenol, which is known for being an aromatic compound with a phenolic structure capable of stabilizing free radicals through electronic delocalization (F. Chen et al., 2009; Mouro et al., 2019). In addition, the presence of CS-MTBAQ introduces further structural and electronic modifications that could enhance the antioxidant activity of the scaffold (Agili, 2024; Kashyap et al., 2012).

The results show that the antioxidant properties of the scaffolds are directly related to the concentration of CS-EU (Fig. 2). In addition, the initial slopes of the scavenging curves suggest that higher CS-EU content and the presence of Nw not only increase the antioxidant capacity but also accelerate the radical neutralization kinetics. This faster response could be beneficial in applications requiring rapid radical elimination (Kang et al., 2017). As the proportion of this derivative increases in the composition, higher DPPH scavenging capacity and faster kinetics are observed, with the plateau being reached between 4 and 7 h.

Notably, regardless of the time required to reach the maximum activity, all scaffolds containing CS-EU or CS-MTBAQ achieve over 90 % of DPPH neutralization. In contrast, the scaffold composed just with CS only reaches 50 % antioxidant activity after 24 h, a value that slightly increases to nearly 60 % with the incorporation of Nw.

Regarding the addition of the nanowhiskers, the same general trend is maintained in the scaffolds; higher CS-EU content results in enhanced

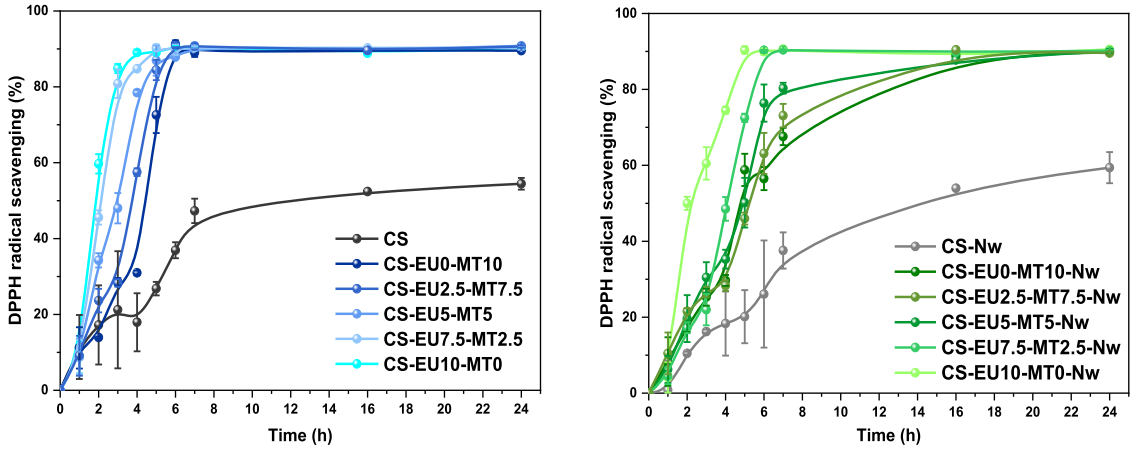

Fig. 2. Antioxidant activity of scaffolds with various compositions of CS-EU and CS-MTBAQ (left), and the addition of Nw (right), $n = 3$.

Table 3
Evaluation of antimicrobial properties of different compositions of scaffolds based on CS.

	S. aureus	*E. faecalis*	*P. aeruginosa*	*E. coli*
CS	75.3 ± 1.1^{a}	-	-	-
CS-EU0-MT10	99.9 ± 0.4^{b}	99.6 ± 0.3^{a}	97.9 ± 1.2^{a}	77.8 ± 3.9^{a}
CS-EU2.5-MT7.5	99.0 ± 0.1^{b}	99.8 ± 0.2^{a}	94.4 ± 3.6^{a}	47.9 ± 3.6^{b}
CS-EU5-MT5	97.4 ± 0.3^{bc}	95.7 ± 1.3^{b}	70.5 ± 3.5^{b}	-
CS-EU7.5-MT2.5	98.1 ± 0.9^{bc}	96.7 ± 1.5^{ab}	67.3 ± 4.8^{bc}	-
CS-EU10-MT0	92.4 ± 3.1^{c}	96.1 ± 1.3^{ab}	-	-
CS-Nw	79.7 ± 0.9^{a}	-	-	-
CS-EU0-MT10-Nw	99.9 ± 0.1^{b}	99.7 ± 2.3^{a}	96.3 ± 2.1^{a}	78.6 ± 2.6^{a}
CS-EU2.5-MT7.5-Nw	99.8 ± 0.1^{b}	99.6 ± 0.3^{a}	93.6 ± 1.8^{a}	49.6 ± 4.2^{b}
CS-EU5-MT5-Nw	99.3 ± 0.2^{b}	97.3 ± 0.6^{ab}	72.4 ± 3.2^{b}	-
CS-EU7.5-MT2.5-Nw	95.4 ± 3.1^{bc}	94.8 ± 2.2^{b}	60.5 ± 5.4^{c}	-
CS-EU10-MT0-Nw	94.4 ± 2.5^{bc}	96.1 ± 0.6^{ab}	-	-

Values having the same letter are not significantly different for the Tukey test (Significance level of $P \leq 0.05$).

antioxidant activity. However, the incorporation of Nw seems to slow down the antioxidant response; the time required to reach the plateau is significantly longer than the scaffolds without Nw, ranging from 8 h to 16 h.

3.3. Antimicrobial properties

The antimicrobial properties of the scaffolds with different compositions were evaluated to assess their ability to inhibit bacterial growth. The purpose was to determine how the incorporation of CS derivatives (CS-EU and CS-MTBAQ) influences the antimicrobial activity of the scaffolds against Gram-positive and Gram-negative bacteria. Since these scaffolds are designed for biomedical applications, it is crucial to understand their behavior in the presence of pathogenic microorganisms, as bacterial contamination could compromise tissue regeneration or lead to infections after implantation.

Four bacteria commonly found in biomaterial-related infections were chosen: *S. aureus, E. faecalis, P. aeruginosa* and *E. coli*. Each scaffold was individually incubated with the corresponding bacterial suspension, and the results are shown in Table 3.

It is clearly seen for all the tested scaffolds that the antibacterial response was notably more effective against the Gram-positive bacteria, *S. aureus* and *E. faecalis*, which are considered in general more susceptible than Gram-negative bacteria primary due to the structural differences in their cell walls. Also, the results revealed that the incorporation of the eugenol and thiazolium-CS derivatives into the polymeric matrix of the scaffolds provides additional biocidal effects to chitosan. It is observed a clear dependence of the antimicrobial activity on the scaffold composition. In all cases, if the content of the CS-MTBAQ decreased and the CS-EU increased, the antibacterial efficacy was reduced. This trend was consistent across all bacterial strains tested. Previous studies have shown that films based on chitosan loaded with eugenol exhibit slightly improved antimicrobial activity compared to plain chitosan, depending on how it is incorporated into the material (Antunes et al., 2021; Muñoz-Bonilla et al., 2019). The antimicrobial effect observed with the scaffolds containing higher proportion of CS-MTBAQ is notably stronger than when CS-EU is in a higher amount. This enhanced activity can be attributed to the permanent positive charges of the quaternized thiazolium groups, which facilitate stronger electrostatic interactions with the negatively charged bacterial membranes, leading to membrane disruption and bacterial death (Alvarez-Paino et al., 2016; Tejero et al., 2015). Therefore, the presence of thiazolium moieties in the CS-MTBAQ structure significantly enhances antimicrobial activity, whereas the contribution of eugenol, despite its known antimicrobial effects, is less effective in this scaffold configuration, possibly due to a lower accessibility from the polymeric matrix.

3.4. Interactions of scaffolds and cells

An essential property in the design of scaffolds for biomedical applications is their protein adsorption capacity. This feature is known to modulate the initial cellular response by facilitating cell growth on the material surface. Efficient protein adsorption could promote cell adhesion and proliferation, as well as support subsequent biological processes such as angiogenesis or bone deposition (Schmidt et al., 2009). In this context, the ability of the scaffold to adsorb proteins was quantified using the BCA assay, aiming to correlate this property with the structure and chemical functionalization of the evaluated CS scaffolds (Cuy et al., 2003; Depan & Misra, 2013). The results are presented in Fig. 4a, where no significant differences or clear trends were observed to indicate whether the scaffold's chemical composition affects protein adsorption, which remains within a range of 60–80 μg/mL. As no significant differences were observed in protein adsorption between the different scaffold compositions, and all of them demonstrated an adequate capacity to support initial cell attachment, these materials can be considered suitable substrates for promoting cell viability and growth.

Therefore, the behavior of NHDFs cultured on the scaffolds was

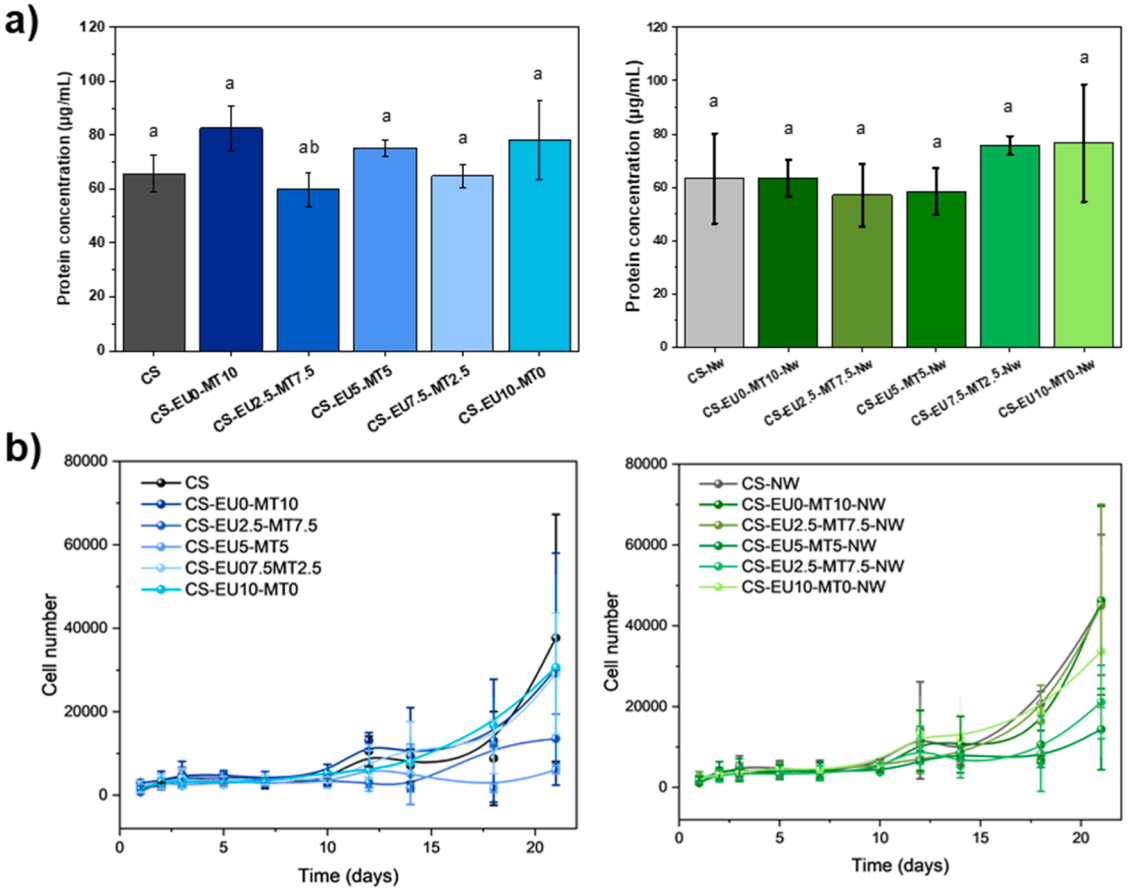

Fig. 4. Fibroblast adhesion and proliferation. (a) Adsorbed protein levels on the surface of scaffolds with different compositions of CS-EU and CS-MTBAQ, $n = 3$. (b) Proliferation of NHDF over time in contact with the scaffolds, $n = 3$. For both parameters, scaffolds are grouped into two sets: with (right) and without Nw (left), shown in separate graphs to facilitate comparison.

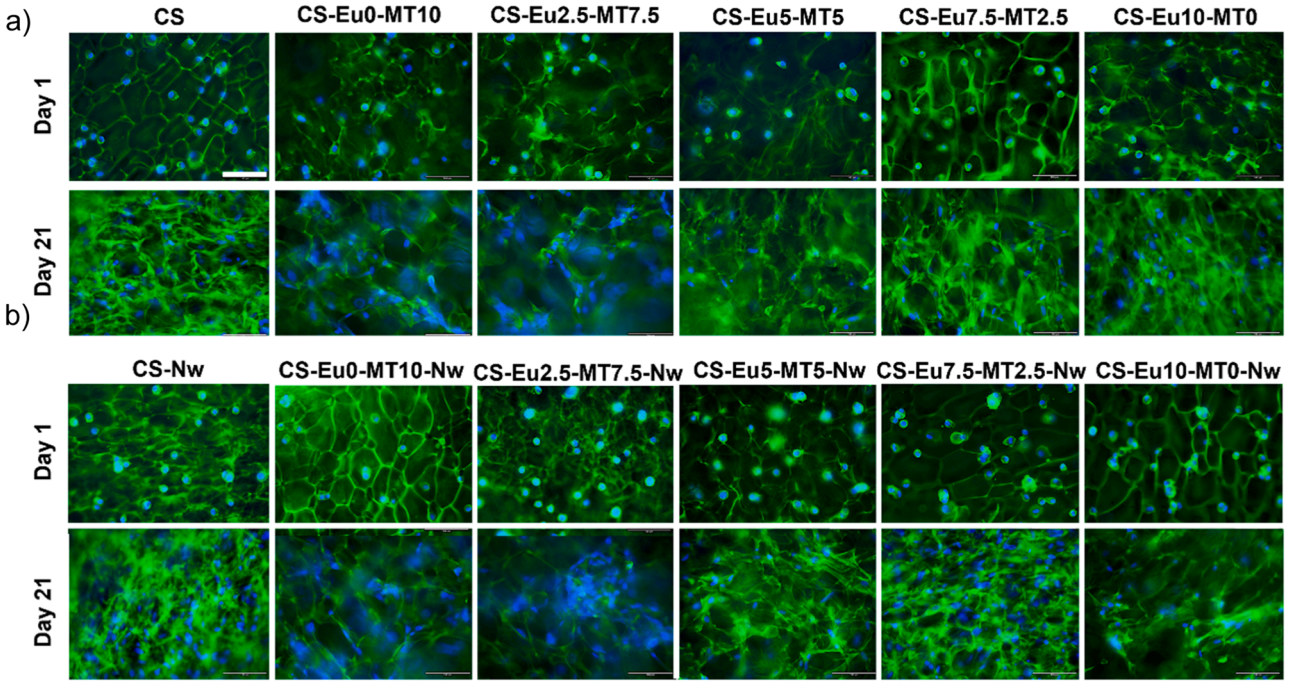

Fig. 5. Characterization of fibroblast morphology on the scaffolds. Representative fluorescence microscopy images of NHDF cultured on different scaffold compositions (a) with or (b) without Nw (green: actin cytoskeleton stained with phalloidin; blue: nuclei stained with DAPI) (Day 1 and Day 21). Representative fluorescence images of fibroblasts show changes in cell morphology and density over time. Scale bar: 100 µm.

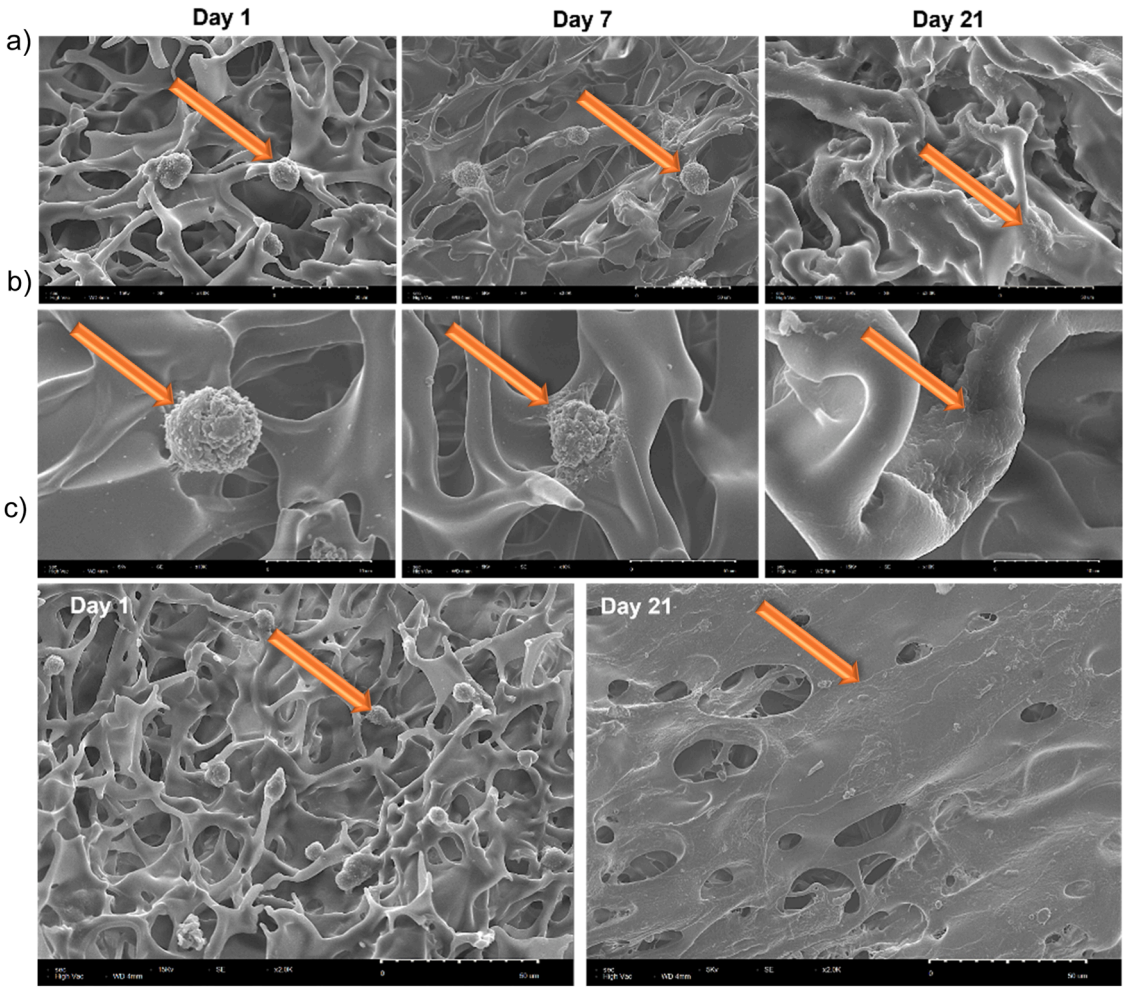

Fig. 6. SEM analysis of fibroblast morphology on the scaffolds. (a) Images of scaffold cross-sections at days 1, 7 and 21, showing cellular morphology and interaction with the porous structure at 3.0 k; (b) SEM images at days 1, 7 and 21 at 10.0k; (c) SEM images of the top surface of the scaffolds at days 1 and 21, illustrating progressive surface coverage.

evaluated to determine their ability to support cell proliferation over time. This analysis provides the relationship between the physicochemical properties of the scaffolds and their impact on the biological response.

The proliferation of NHDF cells on the different scaffolds was assessed using the AlamarBlue assay, which measures cellular metabolic activity as an indicator of viability and proliferation. Two independent experiments were conducted: one with a 7-day time course and another extended to 21 days, allowing the observation of both initial adhesion and early growth as well as proliferation (Bhat & Kumar 2012).

The results showed that fibroblasts were able to proliferate on all scaffold types during the evaluation time, confirming the biocompatibility of the materials (Fig. 4b). No statistically significant differences were found in the proliferation rate among the different scaffolds, which is consistent with the protein adsorption data. These findings support that the chemical variations in the scaffolds do not negatively affect their ability to support cell attachment and proliferation.

The metabolic activity measured in the cells was increased progressively during the first two weeks and almost reached a plateau between days 14 and 21. This behavior is characteristic of cell cultures approaching confluence or reaching a balance in proliferation rate. However, the average metabolic activity remained higher on day 21, suggesting that the trend might still be increasing. It cannot be excluded that the observed variation is due to differences in cell distribution and scaffold colonization. Given the 3D structure, variability in available surface area and pore connectivity influences the ability of cells to migrate and proliferate throughout the scaffold. These results indicate that the scaffolds support initial cell attachment and provide a favorable environment for the sustained proliferation of fibroblasts over prolonged periods, which is an essential feature for tissue engineering applications.

3.5. Cell morphology

On day 1, cells appeared sparsely distributed across the scaffold with a rounded morphology, indicating slow initial adhesion (Asghari Sana et al., 2017; Nwe et al., 2009; Pezeshki-Modaress et al., 2018; Samal et al., 2014) (Fig. 5a). A similar distribution was observed on day 3, although some cells began to spread slightly **(Fig. S1)**.

By day 7, most fibroblasts adopted an elongated morphology, characteristic of cell spreading and cytoskeletal tension organization, although no significant increase in cell number was evident at that stage **(Fig. S1)**. From day 14, the number of nuclei increased notably, suggesting the initiation of a proliferative phase **(Fig. S1)**, which became more pronounced by day 21, where a marked increase in cell density was observed (Fig. 5b). These observations are consistent with the metabolic activity trends previously measured by the Alamar Blue assay, indicating an active proliferation and viability of the cells within the scaffolds over time.

It can be appreciated that the scaffolds exhibited green

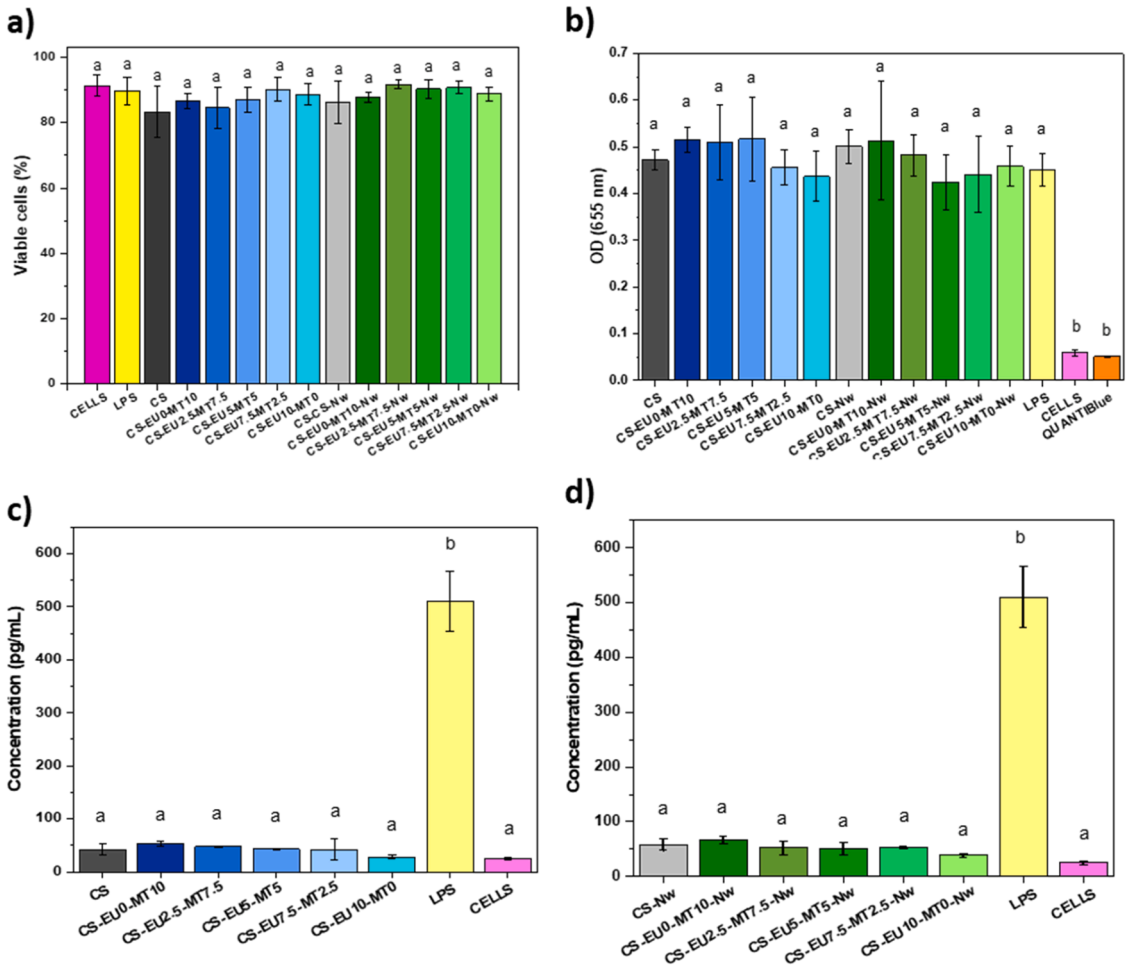

Fig. 7. Evaluation of macrophage response to the different scaffold compositions. (a) Cell viability percentage calculated from fluorescence images, $n = 3$. (b) NF-κB pathway activation assessed via SEAP expression in macrophages after 24 h of scaffold contact (controls: LPS-treated cells as positive, untreated cells as negative, and QuantiBlue reagent as blank), $n = 3$. (c) IL-6 levels measured in the supernatant after 24 h of incubation with the scaffolds with, and (d) without nanowhiskers, (positive control: LPS; negative control: untreated macrophages), $n = 3$.

autofluorescence, due to genipin crosslinking, which partially overlapped with the phalloidin-iFluor-488 green signal. Despite this background fluorescence, cell morphology remained distinguishable in most samples. Additionally, the nuclei stained with DAPI emitted a clear blue signal, allowing accurate identification and localization of cells within the scaffolds.

The scaffolds with the cells at 1,7 and 21 days were dried and analyzed by SEM (Fig. 6a and b), which also provides information of the cellular morphology on the scaffolds over time (Z. Li & Zhang, 2005). On day 1, cells appeared mostly rounded and adhered to the scaffold surface without evident spreading. After 7 days, cells exhibited a more elongated morphology with numerous cytoplasmic extensions interacting with the matrix, suggesting active adhesion. By day 21, cells were extensively spread and showed intimate contact with the scaffold surface (Chu et al., 2009). Additionally, SEM images from the top surface of the scaffolds revealed a similar evolution, depending on the incubation time (Fig. 6c). On day 1, cells were sparsely distributed and had a rounded morphology. In contrast, by day 21, the fibroblasts had proliferated and formed a continuous layer, which covered the entire surface of the scaffold, indicative of effective colonization and extracellular matrix deposition (Heinemann et al., 2008).

Indeed, the viscoelasticity of the scaffolds have an impact on subsequent biological responses, such as cell adhesion, migration, proliferation, and differentiation (Chaudhuri et al., 2020). However, in our case, the differences measured in the stiffness of the scaffolds were not sufficient to observe differences in the initial cell adhesion and subsequent migration and proliferation. Stiffness measured of few kPa or less are considered soft, which typically favors a lower adhesive state of the cell (low integrin expression), with more rounded cell conformations (Engler et al., 2006; Zhan, 2020). In this range, ligand density and conformation might play a bigger role than the mechanical properties of the scaffold as force transmission to the cytoskeleton in response to substrate stiffness only happens above a certain threshold (5 kPa) (Elosegui-Artola et al., 2016). Considering that the scaffolds swell similarly and absorb similar amount of ECM proteins, it was expected a similar initial cell adhesion. After a few days in culture, the influence of the extracellular matrix deposited by the cells drives the proliferation of the fibroblasts.

3.6. *Immune response to scaffolds*

The immune response is also a critical factor in the development of scaffolds for biomedical applications, as these materials can trigger unexpected activation of the immune system, leading to uncontrolled release of proinflammatory cytokines (Vasconcelos et al., 2013). To assess the potential immune reaction caused by the scaffolds, the behavior of macrophages in contact with the different materials was studied, focusing on their activation and viability.

All the synthesized scaffolds were incubated with macrophages for 24 h. After incubation, the culture medium was collected for subsequent

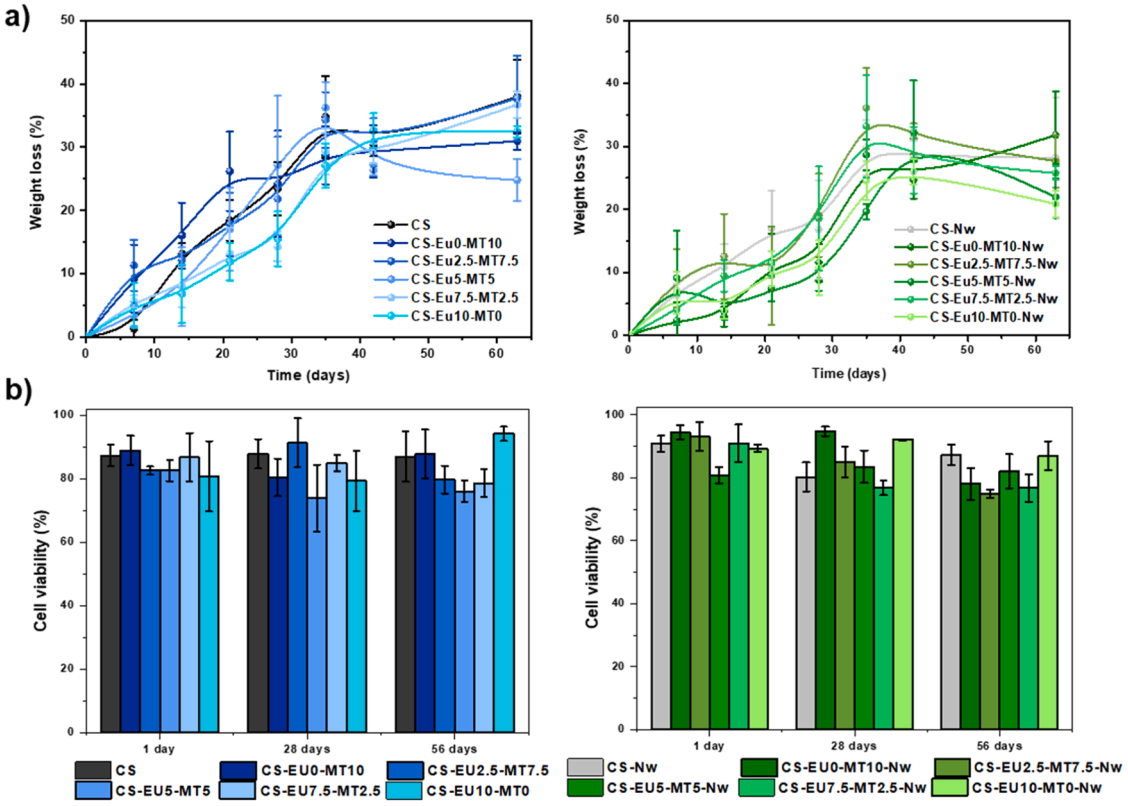

Fig. 8. Biodegradability and cytotoxicity of scaffold degradation. (a) Biodegradation of CS scaffolds, percentage of scaffold weight loss over time following lysozyme treatment, indicating biodegradability, $n = 3$. (b) Cell viability (%) after exposure to scaffold degradation products collected on days 1, 28, and 63, used to assess potential cytotoxic effects, $n = 3$. Scaffold compositions with and without Nw are shown in separate graphs for clarity.

analysis, and Live/Dead assay was performed to evaluate macrophage viability (Jithendra et al., 2024) **(Fig. S2)**. The results showed high cell viability in all groups (Fig. 7a), with approximately 90 % of cells remaining viable, indicating that the scaffolds do not present evident cytotoxic effects on macrophages under these conditions.

NF-κB pathway activation was assessed via the measurement of SEAP, a phosphatase that is genetically encoded to be released upon NF-κB activation. NF-κB is a transcription factor that is known for regulating immune and inflammatory responses. When macrophages recognize a potentially harmful stimuli, such as pathogens or foreign materials, these cells activate NF-κB signaling, activating a downstream signaling cascade of various proinflammatory genes (Y. Li et al., 2017). The results of the SEAP quantification revealed significant activation of NF-κB in the medium in presence of the scaffolds (Fig. 7b). Lipopolysaccharides (LPS), known by being a potent activator of macrophages, were used as a positive control, and unstimulated macrophages served as the negative control (Hyun et al., 2017). The SEAP levels detected in the media exposed to the scaffolds were comparable to those of the positive control, suggesting that the scaffolds are capable of activating the NF-κB pathway under these experimental conditions.

Among all the cytokines secreted by activated macrophages, IL-6 has a prominent role in modulating inflammation and promoting immune cell infiltration to the tissue during inflammation (Fig. 7c and d). To quantify IL-6 secretion, an ELISA was performed using the same positive (LPS) and negative (unstimulated cells) controls (Shen et al., 2020). Despite the activation observed in the NF-κB pathway, IL-6 concentrations in the media from the scaffolds incubated with cells remained moderate. The values were closer to those of the negative control.

These results indicate that, although the scaffolds induce partial activation of macrophages via the NF-κB pathway, the inflammatory response in terms of IL-6 production is limited. This suggests a controlled immune activation and supports the potential biocompatibility of these scaffolds for biomedical use.

3.7. *In vitro biodegradation*

The evaluation of scaffold degradation under enzymatic conditions provides valuable information about the stability and durability of the materials planned for biomedical applications (Han et al., 2012). In this study, a lysozyme solution derived from egg white (13 mg/L in PBS) was employed to simulate the physiological environment that the scaffolds would find in the body (Lončarević et al., 2017).

As shown in Fig. 8, all scaffolds exhibited a slow and gradual enzymatic degradation during the first weeks. This moderate loss of weight can be attributed to the structural reinforcement provided by genipin, which acts as a crosslinking agent and limits the enzymatic accessibility of the CS polymer chains (Q. Q. Li et al., 2015; Vo et al., 2021).

In addition, no statistically significant differences were observed among the different scaffold formulations regarding their degradation profiles, indicating that scaffold composition would not have a decisive effect on the degradation rate. Similarly, variations in the porosity do not appear to substantially affect the degradation process. This suggests that the crosslinking effect of genipin is the dominant factor. Although the results are not statistically significant, scaffolds reinforced with Nw exhibited a slight trend toward increased resistance to degradation, which could indicate an enhanced resistance to enzymatic degradation (M. Liu et al., 2025).

The chemical modification of CS did not accelerate its enzymatic degradation, remaining comparable to previously reported genipin-crosslinked CS scaffolds (Y.-H. Q. Li et al., 2015; Mak & Leung, 2019). This slow degradation profile is advantageous for tissue regeneration, where prolonged scaffold stability is often required. Moreover, the incorporation of reinforcing agents did not significantly alter the degradation rate. In contrast, other studies incorporating materials such

as hydroxyapatite, tricalcium phosphate, or cellulose nanoparticles have reported increased degradation, likely due to changes in scaffold structure and porosity that facilitate enzyme and fluid penetration (Azaman et al., 2022; Patel et al., 2022; Qasim et al., 2017).

The progressive degradation of the scaffolds could lead to the release of products into the medium, which would interact with cells in a biological environment. For this reason, it is important to analyze the medium collected at different times during the enzymatic assay, as it could contain degradation residues that would affect cell behavior. The cytocompatibility of these media was further evaluated by performing an MTT assay on NHDFs exposed to the degradation media collected on days 1, 28, and 63, representing the early, intermediate, and late stages of the biodegradation process. In all cases, cell viability values remained above 80 %, confirming the non-cytotoxic nature of the compounds released during scaffold degradation. These findings support the suitability of the developed materials for long-term use in biomedical applications, where sustained degradation and high biocompatibility are required.

4. Conclusions

We have demonstrated that CS scaffolds were successfully prepared with different ratios of CS-EU and CS-MTBAQ with a total of 10 wt % and 1 wt % of Nws, achieving antioxidant and antimicrobial properties without compromising the structural integrity or mechanical stability. Cell adhesion, spreading and proliferation confirmed the biocompatibility of all scaffold types. In terms of immunological response, the scaffolds did not trigger a strong proinflammatory reaction, as indicated by the absence of a cytokine release cascade. However, a moderate immune response was observed, implying that these materials are bioactive and capable of interacting with the host immune system without eliciting adverse effects. Their favorable immunological profile and ability to sustain fibroblast proliferation highlight their promise for future application in soft tissue engineering.

CRediT authorship contribution statement

C. Muñoz-Núñez: Writing – original draft, Investigation, Formal analysis, Data curation. **A. Barco-Martín:** Investigation, Formal analysis. **K. Deshpande:** Investigation, Formal analysis. **D.S. Schmidt:** Investigation, Formal analysis. **L. González-García:** Writing – review & editing, Investigation, Formal analysis. **S. Trujillo:** Writing – review & editing, Project administration, Funding acquisition, Conceptualization. **A. Muñoz-Bonilla:** Writing – review & editing, Supervision, Project administration, Investigation, Funding acquisition, Conceptualization. **M. Fernández-García:** Writing – review & editing, Supervision, Project administration, Investigation, Funding acquisition, Conceptualization.

Declaration of competing interest

The authors declare that they have no known competing financial interests or personal relationships that could have appeared to influence the work reported in this paper.

Acknowledgements

This work was financially supported by the MICIU (PID2022–13651OB-100), the Agencia Estatal de Investigación (AEI, Spain) and Fondo Europeo de Desarrollo Regional (FEDER, EU). C. Muñoz-Núñez acknowledges MICINN for her FPI fellowship PRE2020–093596. S. Trujillo thanks Pharmaceutical Research Allianz Saarland (Pharma Science Hub) for funding.

Supplementary materials

Supplementary material associated with this article can be found, in the online version, at doi:10.1016/j.carpta.2025.101069.

Data availability

Data will be made available on request.

References

Abbasi, N., Hamlet, S., Love, R. M., & Nguyen, N.-T. (2020). Porous scaffolds for bone regeneration. *Journal of Science: Advanced Materials and Devices, 5*(1), 1–9. https://doi.org/10.1016/j.jsamd.2020.01.007

Abourehab, M. A. S., Pramanik, S., Abdelgawad, M. A., Abualsoud, B. M., Kadi, A., Ansari, M. J., & Deepak, A. (2022). Recent advances of Chitosan formulations in biomedical applications. *International Journal of Molecular Sciences, 23*(18), Article 10975. https://doi.org/10.3390/ijms231810975

Agili, F. (2024). Novel thiazole derivatives containing imidazole and furan scaffold: Design, synthesis, molecular docking, antibacterial, and antioxidant evaluation. *Molecules (Basel, Switzerland), 29*(7), 1491. https://doi.org/10.3390/molecules29071491

Almeida lima, Â. M., Moreira, L. C., Gazolla, P. R., Oliveira, M. B., Teixeira, R. R., Queiroz, V. T., Rocha, M. R., Moraes, W. B., dos Santos, N. A., Romão, W., Lacerda, V., Bezerra Morais, P. A., Oliveira, O. V.de, Júnior, W. C.de J., Barbosa, L. C. A., Nascimento, C. J., Junker, J., & Costa, A. V (2024). Design and synthesis of eugenol derivatives bearing a 1,2,3-triazole moiety for Papaya protection against colletotrichum gloeosporioides. *Journal of Agricultural and Food Chemistry, 72*(22), 12459–12468. https://doi.org/10.1021/acs.jafc.4c00440

Alvarez-Paino, M., Juan-Rodríguez, R., Cuervo-Rodríguez, R., Tejero, R., López, D., López-Fabal, F., Gómez-Garcés, J. L., Muñoz-Bonilla, A., & Fernández-García, M. (2016). Antimicrobial films obtained from latex particles functionalized with quaternized block copolymers. *Colloids and Surfaces B: Biointerfaces*, 140. https://doi.org/10.1016/j.colsurfb.2015.12.031

Antunes, J. C., Tavares, T. D., Teixeira, M. A., Teixeira, M. O., Homem, C., Amorim, M. T. P., & Felgueiras, H. P. (2021). Eugenol-containing essential oils loaded onto Chitosan polyvinyl alcohol blended films and their ability to eradicate Staphylococcus aureus or Pseudomonas aeruginosa from infected microenvironments. *Pharmaceutics, 13*, 195.

Asghari Sana, F., Çapkın Yurtsever, M., Kaynak Bayrak, G., Tunçay, E.Ö., Kiremitçi, A. S., & Gümüşderelioğlu, M. (2017). Spreading, proliferation and differentiation of human dental pulp stem cells on chitosan scaffolds immobilized with RGD or fibronectin. *Cytotechnology, 69*(4), 617–630. https://doi.org/10.1007/s10616-017-0072-9

Azaman, F. A., Zhou, K., Blanes-Martínez, M., del, M., Brennan Fournet, M., & Devine, D. M. (2022). Bioresorbable chitosan-based bone regeneration scaffold using various bioceramics and the alteration of photoinitiator concentration in an extended UV photocrosslinking reaction. *Gels (Basel, Switzerland), 8*(11), 696. https://doi.org/10.3390/gels8110696

Bai, L., Liu, L., Esquivel, M., Tardy, B. L., Huan, S., Niu, X., Liu, S., Yang, G., Fan, Y., & Rojas, O. J. (2022). Nanochitin: Chemistry, structure, assembly, and applications. *Chemical Reviews, 122*(13), 11604–11674. https://doi.org/10.1021/acs.chemrev.2c00125

Bernkop-Schnürch, A., & Dünnhaupt, S. (2012). Chitosan-based drug delivery systems. *European Journal of Pharmaceutics and Biopharmaceutics, 81*(3), 463–469. https://doi.org/10.1016/j.ejpb.2012.04.007

Bhat, S., & Kumar, A. (2012). Cell proliferation on three-dimensional chitosan–agarose–gelatin cryogel scaffolds for tissue engineering applications. *Journal of Bioscience and Bioengineering, 114*(6), 663–670. https://doi.org/10.1016/j.jbiosc.2012.07.005

Borges-Vilches, J., Unalan, I., Aguayo, C. R., Fernández, K., & Boccaccini, A. R. (2023). Multifunctional Chitosan scaffold platforms loaded with natural polyphenolic extracts for wound dressing applications. *Biomacromolecules, 24*(11), 5183–5193. https://doi.org/10.1021/acs.biomac.3c00727

Chaudhuri, O., Cooper-White, J., Janmey, P. A., Mooney, D. J., & Shenoy, V. B. (2020). Effects of extracellular matrix viscoelasticity on cellular behaviour. *Nature, 584*(7822), 535–546. https://doi.org/10.1038/s41586-020-2612-2

Chen, F., Shi, Z., Neoh, K. G., & Kang, E. T. (2009). Antioxidant and antibacterial activities of eugenol and carvacrol-grafted chitosan nanoparticles. *Biotechnology and Bioengineering, 104*(1), 30–39. https://doi.org/10.1002/bit.22363

Chen, Q., Qi, Y., Jiang, Y., Quan, W., Luo, H., Wu, K., Li, S., & Ouyang, Q. (2022). Progress in research of Chitosan chemical modification technologies and their applications. *Marine Drugs, 20*(8), 536. https://doi.org/10.3390/md20080536

Chi-Yan Li, S., Sun, Y.-C., Guan, Q., & Naguib, H. (2016). Effects of chitin nanowhiskers on the thermal, barrier, mechanical, and rheological properties of polypropylene nanocomposites. *RSC Advances, 6*(76), 72086–72095. https://doi.org/10.1039/C6RA11623J

Chiloeches, A., Cuervo-Rodríguez, R., López-Fabal, F., Fernández-García, M., Echeverría, C., & Muñoz-Bonilla, A. (2022). Antibacterial and compostable polymers derived from biobased itaconic acid as environmentally friendly additives for biopolymers. *Polymer Testing, 109*, Article 107541. https://doi.org/10.1016/j.polymertesting.2022.107541

Chu, X.-H., Shi, X.-L., Feng, Z.-Q., Gu, Z.-Z., & Ding, Y.-T. (2009). Chitosan nanofiber scaffold enhances hepatocyte adhesion and function. *Biotechnology Letters, 31*(3), 347–352. https://doi.org/10.1007/s10529-008-9892-1

Ciarlantini, C., Garcia, R. B., Lacolla, E., Francolini, I., Fernández-García, M., Nuñez, C. M., Bonilla, A. M., & Piozzi, A. (2025). Nanofibrous scaffolds based on

polyelectrolyte complexes of chitosan-alginate-COLLAGEN and chitosan-hyaluronic acid for tissue engineering. *Carbohydrate Polymer Technologies and Applications*, (June), 11. https://doi.org/10.1016/j.carpta.2025.100915

Ciarlantini, C., Lacolla, E., Francolini, I., Fernández-García, M., Muñoz-Núñez, C., Muñoz-Bonilla, A., & Piozzi, A. (2024). Development of antioxidant and antimicrobial membranes based on functionalized and crosslinked chitosan for tissue regeneration. *International Journal of Molecular Sciences, 25*(4). https://doi.org/10.3390/ijms25041961

Croisier, F., & Jérôme, C. (2013). Chitosan-based biomaterials for tissue engineering. *European Polymer Journal, 49*(4), 780–792. https://doi.org/10.1016/j.eurpolymj.2012.12.009

Cui, J., Sun, Y., Wang, L., Miao, Q., Tan, W., & Guo, Z. (2022). Preparation of L-arginine schiff bases modified chitosan derivatives and their antimicrobial and antioxidant properties. *Marine Drugs, 20*(11), 688. https://doi.org/10.3390/md20110688

Cuy, J. L., Beckstead, B. L., Brown, C. D., Hoffman, A. S., & Giachelli, C. M. (2003). Adhesive protein interactions with chitosan: Consequences for valve endothelial cell growth on tissue-engineering materials. *Journal of Biomedical Materials Research Part A, 67A*(2), 538–547. https://doi.org/10.1002/jbm.a.10095

Dash, D. R., Singh, S. K., & Singha, P. (2024). International Journal of Biological Macromolecules viscoelastic behavior, gelation properties and structural characterization of Deccan hemp seed (Hibiscus cannabinus) protein : Influence of protein and ionic concentrations, pH, and temperature. *International Journal of Biological Macromolecules, 263*(P1), Article 130120. https://doi.org/10.1016/j.ijbiomac.2024.130120

Dash, M., Chiellini, F., Ottenbrite, R. M., & Chiellini, E. (2011). Chitosan—A versatile semi-synthetic polymer in biomedical applications. *Progress in Polymer Science, 36*(8), 981–1014. https://doi.org/10.1016/j.progpolymsci.2011.02.001

Dawood, K. M., Eldebss, T. M. A., El-Zahabi, H. S. A., Yousef, M. H., & Metz, P. (2013). Synthesis of some new pyrazole-based 1,3-thiazoles and 1,3,4-thiadiazoles as anticancer agents. *European Journal of Medicinal Chemistry, 70*, 740–749. https://doi.org/10.1016/j.ejmech.2013.10.042

Depan, D., & Misra, R. D. K. (2013). The interplay between nanostructured carbon-grafted chitosan scaffolds and protein adsorption on the cellular response of osteoblasts: Structure–function property relationship. *Acta Biomaterialia, 9*(4), 6084–6094. https://doi.org/10.1016/j.actbio.2012.12.019

Ding, X., Tang, Q., Xu, Z., Xu, Y., Zhang, H., Zheng, D., Wang, S., Tan, Q., Maitz, J., Maitz, P. K., Yin, S., Wang, Y., & Chen, J. (2022). Challenges and innovations in treating chronic and acute wound infections: From basic science to clinical practice. *Burns and Trauma, 10*. https://doi.org/10.1093/burnst/tkac014

Drozdova, M., Vodyakova, M., Tolstova, T., Chernogortseva, M., Sazhnev, N., Demina, T., Aksenova, N., Timashev, P., Kildeeva, N., & Markvicheva, E. (2023). Composite hydrogels based on cross-linked chitosan and low molecular weight hyaluronic acid for tissue engineering. *Polymers, 15*(10), 2371. https://doi.org/10.3390/polym15102371

Elosegui-Artola, A., Oria, R., Chen, Y., Kosmalska, A., Pérez-González, C., Castro, N., Zhu, C., Trepat, X., & Roca-Cusachs, P. (2016). Mechanical regulation of a molecular clutch defines force transmission and transduction in response to matrix rigidity. *Nature Cell Biology, 18*(5), 540–548. https://doi.org/10.1038/ncb3336

Engler, A. J., Sen, S., Sweeney, H. L., & Discher, D. E. (2006). Matrix elasticity directs stem cell lineage specification. *Cell, 126*(4), 677–689. https://doi.org/10.1016/j.cell.2006.06.044

Fabiano, A., Beconcini, D., Migone, C., Piras, A. M., & Zambito, Y. (2020). Quaternary Ammonium Chitosans: The importance of the positive fixed charge of the drug delivery systems. *International Journal of Molecular Sciences, 21*(18), 6617. https://doi.org/10.3390/ijms21186617

Fadilah, N. I. M., Phang, S. J., Kamaruzaman, N., Salleh, A., Zawani, M., Sanyal, A., Maarof, M., & Fauzi, M. B. (2023). Antioxidant biomaterials in cutaneous wound healing and tissue regeneration: A critical review. *Antioxidants*, (4), 12. https://doi.org/10.3390/antiox12040787

Florczyk, S. J., Wang, K., Jana, S., Wood, D. L., Sytsma, S. K., Sham, J. G., Kievit, F. M., & Zhang, M. (2013). Porous chitosan-hyaluronic acid scaffolds as a mimic of glioblastoma microenvironment ECM. *Biomaterials, 34*(38), 10143–10150. https://doi.org/10.1016/j.biomaterials.2013.09.034

Gao, X., Xu, Z., Liu, G., & Wu, J. (2021). Polyphenols as a versatile component in tissue engineering. *Acta Biomaterialia, 119*, 57–74. https://doi.org/10.1016/j.actbio.2020.11.004

Gaweł, J., Milan, J., Żebrowski, J., Płoch, D., Stefaniuk, I., & Kus-Liśkiewicz, M. (2023). Biomaterial composed of chitosan, riboflavin, and hydroxyapatite for bone tissue regeneration. *Scientific Reports, 13*(1), Article 17004. https://doi.org/10.1038/s41598-023-44225-0

Gholap, A. D., Rojekar, S., Kapare, H. S., Vishwakarma, N., Raikwar, S., Garkal, A., Mehta, T. A., Jadhav, H., Prajapati, M. K., & Annapure, U. (2024). Chitosan scaffolds: Expanding horizons in biomedical applications. *Carbohydrate Polymers, 323*, Article 121394. https://doi.org/10.1016/j.carbpol.2023.121394

Griffon, D., Sedighi, M., Schaeffer, D., Eurell, J., & Johnson, A. (2006). Chitosan scaffolds: Interconnective pore size and cartilage engineering. *Acta Biomaterialia, 2*(3), 313–320. https://doi.org/10.1016/j.actbio.2005.12.007

Han, T., Nwe, N., Furuike, T., Tokura, S., & Tamura, H. (2012). Methods of N-acetylated chitosan scaffolds and its in vitro biodegradation by lysozyme. *Journal of Biomedical Science and Engineering, 05*(01), 15–23. https://doi.org/10.4236/jbise.2012.51003

Heinemann, C., Heinemann, S., Bernhardt, A., Worch, H., & Hanke, T. (2008). Novel textile Chitosan scaffolds promote spreading, proliferation, and differentiation of osteoblasts. *Biomacromolecules, 9*(10), 2913–2920. https://doi.org/10.1021/bm800693d

Hing, K. A., Annaz, B., Saeed, S., Revell, P. A., & Buckland, T. (2005). Microporosity enhances bioactivity of synthetic bone graft substitutes. *Journal of Materials Science: Materials in Medicine, 16*(5), 467–475. https://doi.org/10.1007/s10856-005-6988-1

Homayoni, H., Ravandi, S. A. H., & Valizadeh, M. (2009). Electrospinning of chitosan nanofibers: Processing optimization. *Carbohydrate Polymers, 77*(3), 656–661. https://doi.org/10.1016/j.carbpol.2009.02.008

Huang, Y., Seitz, D., König, F., Müller, P. E., Jansson, V., & Klar, R. M. (2019). Induction of articular chondrogenesis by Chitosan/hyaluronic-acid-based biomimetic matrices using Human adipose-derived stem cells. *International Journal of Molecular Sciences, 20*(18), 4487. https://doi.org/10.3390/ijms20184487

Hyun, H., Hashimoto-Hill, S., Kim, M., Tsifansky, M. D., Kim, C. H., & Yeo, Y. (2017). Succinylated Chitosan derivative has local protective effects on intestinal inflammation. *ACS Biomaterials Science & Engineering, 3*(8), 1853–1860. https://doi.org/10.1021/acsbiomaterials.7b00262

Ibrahim, A. G., Fouda, A., Elgammal, W. E., Eid, A. M., Elsenety, M. M., Mohamed, A. E., & Hassan, S. M. (2022). New thiadiazole modified chitosan derivative to control the growth of human pathogenic microbes and cancer cell lines. *Scientific Reports, 12*(1), Article 21423. https://doi.org/10.1038/s41598-022-25772-4

Jiankang, H., Dichen, L., Yaxiong, L., Bo, Y., Bingheng, L., & Qin, L. (2007). Fabrication and characterization of chitosan/gelatin porous scaffolds with predefined internal microstructures. *Polymer, 48*(15), 4578–4588. https://doi.org/10.1016/j.polymer.2007.05.048

Jiménez-Gómez, C. P., & Cecilia, J. A. (2020). Chitosan: A natural biopolymer with a wide and varied range of applications. *Molecules (Basel, Switzerland), 25*(17), 3981. https://doi.org/10.3390/molecules25173981

Jithendra, P., Annamalai, D., Ebrahim, H. A., Ibrahim, A. M., El-Sherbiny, M., Rajam, A. M., EL-Nablaway, M., & Mohamed, J. M. M. (2024). Bioassessment of the inflammatory response of macrophages to collagen-chitosan scaffold blended with Aloe vera. *Biomass Conversion and Biorefinery, 14*(20), 25045–25055. https://doi.org/10.1007/s13399-023-04535-9

Jung, B., Chung, S., & Lee, S. B. (2006). Preparation and characterization of eugenol-grafted chitosan hydrogels and their antioxidant activities. *Journal of Applied Polymer Science, 99*(6), 3500–3506. https://doi.org/10.1002/app.22974

Kamarul, T., Krishnamurithy, G., Salih, N. D., Ibrahim, N. S., Raghavendran, H. R. B., Suhaeb, A. R., & Choon, D. S. K. (2014). Biocompatibility and toxicity of poly(vinyl alcohol)/N,O-carboxymethyl chitosan scaffold. *The Scientific World Journal, 2014*, 1–7. https://doi.org/10.1155/2014/905103

Kang, B., Vales, T., Cho, B.-K., Kim, J.-K., & Kim, H.-J. (2017). Development of gallic acid-modified hydrogels using interpenetrating Chitosan network and evaluation of their antioxidant activity. *Molecules (Basel, Switzerland), 22*(11), 1976. https://doi.org/10.3390/molecules22111976

Kanimozhi, K., Khaleel Basha, S., & Sugantha Kumari, V. (2016). Processing and characterization of chitosan/PVA and methylcellulose porous scaffolds for tissue engineering. *Materials Science and Engineering: C, 61*, 484–491. https://doi.org/10.1016/j.msec.2015.12.084

Karakeçili, A., Korpayev, S., & Orhan, K. (2022). Optimizing chitosan/collagen type I/nanohydroxyapatite cross-linked porous scaffolds for bone tissue engineering. *Applied Biochemistry and Biotechnology, 194*(9), 3843–3859. https://doi.org/10.1007/s12010-022-03962-0

Kashyap, S. J., Garg, V. K., Sharma, P. K., Kumar, N., Dudhe, R., & Gupta, J. K. (2012). Thiazoles: Having diverse biological activities. *Medicinal Chemistry Research, 21*(8), 2123–2132. https://doi.org/10.1007/s00044-011-9685-2

Khadim, H., Zeeshan, R., Riaz, S., Tabassum, S., Ansari, A. A., Zulfiqar, S., Yar, M., & Asif, A. (2024). Development of eugenol loaded cellulose-chitosan based hydrogels; in-vitro and in-vivo evaluation for wound healing. *Colloids and Surfaces A: Physicochemical and Engineering Aspects, 693*, Article 134033. https://doi.org/10.1016/j.colsurfa.2024.134033

Kim, M. S., Park, S. J., Gu, B. K., & Kim, C.-H. (2012). Inter-connecting pores of chitosan scaffold with basic fibroblast growth factor modulate biological activity on human mesenchymal stem cells. *Carbohydrate Polymers, 87*(4), 2683–2689. https://doi.org/10.1016/j.carbpol.2011.11.060

Korpayev, S., & Ahmed, S. I. (2021). Chitosan and silver nanoparticles are attractive auxin carriers : A comparative study on the adventitious rooting of microcuttings in apple rootstocks. *Biotechnology Journal, 16*(January), 1–10. https://doi.org/10.1002/biot.202100046

Korpayev, S., Kaygusuz, G., Şen, M., Orhan, K., Oto, Ç., & Karakeçili, A. (2020a). Chitosan/collagen based biomimetic osteochondral tissue constructs: A growth factor-free approach. *International Journal of Biological Macromolecules, 156*, 681–690. https://doi.org/10.1016/j.ijbiomac.2020.04.109

Korpayev, S., Toprak, Ö., Murat, Ş., & Orhan, K. (2020b). Regulation of chondrocyte hypertrophy in an osteochondral interface mimicking gel matrix. *Colloids and Surfaces B : Biointerfaces*, (January), 193. https://doi.org/10.1016/j.colsurfb.2020.111111

Kowalewska, A., & Majewska-Smolarek, K. (2023). Eugenol-based polymeric materials—Antibacterial activity and applications. *Antibiotics, 12*(11), 1570. https://doi.org/10.3390/antibiotics12111570

Li, D., Gao, H., Li, M., Chen, G., Guan, L., He, M., Tian, J., & Cao, R. (2020). Nanochitin/metal ion dual reinforcement in synthetic polyacrylamide network-based nanocomposite hydrogels. *Carbohydrate Polymers, 236*, Article 116061. https://doi.org/10.1016/j.carbpol.2020.116061

Li, Q., Wang, X., Lou, X., Yuan, H., Tu, H., Li, B., & Zhang, Y. (2015). Genipin-crosslinked electrospun chitosan nanofibers: Determination of crosslinking conditions and evaluation of cytocompatibility. *Carbohydrate Polymers, 130*, 166–174. https://doi.org/10.1016/j.carbpol.2015.05.039

Li, Y., Wang, X., Ren, J., Lan, X., Li, J., Yi, J., Liu, L., Han, Y., Zhang, S., Li, D., & Lu, S. (2017). Identification and application of anti-inflammatory compounds screening

system based on RAW264.7 cells stably expressing NF-κb-dependent SEAP reporter gene. *BMC Pharmacology and Toxicology, 18*(1), 5. https://doi.org/10.1186/s40360-016-0113-6

Li, Z., & Zhang, M. (2005). Chitosan–alginate as scaffolding material for cartilage tissue engineering. *Journal of Biomedical Materials Research Part A, 75A*(2), 485–493. https://doi.org/10.1002/jbm.a.30449

Liu, J., Liu, S., Chen, Y., Zhang, L., Kan, J., & Jin, C. (2017). Physical, mechanical and antioxidant properties of chitosan films grafted with different hydroxybenzoic acids. *Food Hydrocolloids, 71*, 176–186. https://doi.org/10.1016/j.foodhyd.2017.05.019

Liu, M., Cui, Z., Xu, D., Liu, C., & Zhou, C. (2025). Chitin nanocrystal-reinforced chitin/collagen composite hydrogels for annulus fibrosus repair after discectomy. *Materials Today Bio, 31*, Article 101537. https://doi.org/10.1016/j.mtbio.2025.101537

Liu, W., Zu, L., Wang, S., Li, J., Fei, X., Geng, M., Zhu, C., & Shi, H. (2023). Tailored biomedical materials for wound healing. *Burns and Trauma, 11*. https://doi.org/10.1093/burnst/tkad040

Lončarević, A., Ivanković, M., & Rogina, A. (2017). Lysozyme-induced degradation of Chitosan: The characterisation of degraded Chitosan scaffolds. *Journal of Tissue Repair and Regeneration, 1*(1), 12–22. https://doi.org/10.14302/issn.2640-6403.jtrr-17-1840

Mak, Y. W., & Leung, W. W.-F (2019). Crosslinking of genipin and autoclaving in chitosan-based nanofibrous scaffolds: Structural and physiochemical properties. *Journal of Materials Science, 54*(15), 10941–10962. https://doi.org/10.1007/s10853-019-03649-8

Mallakpour, S., Sirous, F., & Hussain, C. M. (2021). Current achievements in 3D bioprinting technology of chitosan and its hybrids. *New Journal of Chemistry, 45*(24), 10565–10576. https://doi.org/10.1039/D1NJ01497H

Marchese, A., Barbieri, R., Coppo, E., Orhan, I. E., Daglia, M., Nabavi, S. F., Izadi, M., Abdollahi, M., Nabavi, S. M., & Ajami, M. (2017). Antimicrobial activity of eugenol and essential oils containing eugenol: A mechanistic viewpoint. *Critical Reviews in Microbiology, 43*(6), 668–689. https://doi.org/10.1080/1040841X.2017.1295225

Martău, G. A., Mihai, M., & Vodnar, D. C. (2019). The use of Chitosan, Alginate, and Pectin in the biomedical and food sector—Biocompatibility, bioadhesiveness, and biodegradability. *Polymers, 11*(11), 1837. https://doi.org/10.3390/polym11111837

Martins, A., Facchi, S., Follmann, H., Pereira, A., Rubira, A., & Muniz, E. (2014). Antimicrobial activity of Chitosan derivatives containing N-quaternized moieties in its backbone: A review. *International Journal of Molecular Sciences, 15*(11), 20800–20832. https://doi.org/10.3390/ijms151120800

Matica, A., Menghiu, G., & Ostafe, V. (2017). Biodegradability of Chitosan based products. *Former: Ann. West Univ. Timisoara-Series Chem, 26*(1), 75–86.

Medeiros Borsagli, F. G. L., Carvalho, I. C., & Mansur, H. S. (2018). Amino acid-grafted and N-acylated chitosan thiomers: Construction of 3D bio-scaffolds for potential cartilage repair applications. *International Journal of Biological Macromolecules, 114*, 270–282. https://doi.org/10.1016/j.ijbiomac.2018.03.133

Mezger, T. (2020). The Rheology Handbook. *For users of rotational and oscillatory rheometers*. Vincentz Network. https://doi.org/10.1515/9783748603702

Miranda, D. G., Malmonge, S. M., Campos, D. M., Attik, N. G., Grosgogeat, B., & Gritsch, K. (2016). A chitosan-hyaluronic acid hydrogel scaffold for periodontal tissue engineering. *Journal of Biomedical Materials Research Part B: Applied Biomaterials, 104*(8), 1691–1702. https://doi.org/10.1002/jbm.b.33516

Mohamed, A. E., Elgammal, W. E., Dawaba, A. M., Ibrahim, A. G., Fouda, A., & Hassan, S. M. (2022). A novel 1,3,4-thiadiazole modified chitosan: Synthesis, characterization, antimicrobial activity, and release study from film dressings. *Applied Biological Chemistry, 65*(1), 54. https://doi.org/10.1186/s13765-022-00725-7

Mohan, K., Ganesan, A. R., Ezhilarasi, P. N., Kondamareddy, K. K., Rajan, D. K., Sathishkumar, P., Rajarajeswaran, J., & Conterno, L. (2022). Green and eco-friendly approaches for the extraction of chitin and chitosan: A review. *Carbohydrate Polymers, 287*, Article 119349. https://doi.org/10.1016/j.carbpol.2022.119349

Mouro, C., Simões, M., & Gouveia, I. C. (2019). Emulsion electrospun Fiber mats of PCL/PVA/chitosan and eugenol for wound dressing applications. *Advances in Polymer Technology, 2019*, 1–11. https://doi.org/10.1155/2019/9859506

Moussian, B. (2019). *Chitin: Structure, chemistry and biology* (pp. 5–18). https://doi.org/10.1007/978-981-13-7318-3_2.

Muñoz-Bonilla, A., Echeverria, C., Sonseca, Á., Arrieta, M. P., & Fernández-García, M. (2019). Bio-based polymers with antimicrobial properties towards sustainable development. *Materials, 12*(4), 641. https://doi.org/10.3390/ma12040641

Muñoz-Nuñez, C., Cuervo-Rodríguez, R., Echeverría, C., Fernández-García, M., & Muñoz-Bonilla, A. (2023). Synthesis and characterization of thiazolium chitosan derivative with enhanced antimicrobial properties and its use as component of chitosan based films. *Carbohydrate Polymers, 302*, 1–11. https://doi.org/10.1016/j.carbpol.2022.120438

Muñoz-Nuñez, C., Fernández-García, M., & Muñoz-Bonilla, A. (2022). Chitin nanocrystals : Environmentally friendly materials for the development of bioactive films. *Coatings, 12*(2), 144.

Muñoz-Núñez, C., Gómez-Fernández, N., Muñoz-Bonilla, A., & Fernández-García, M. (2025). Chemical modification of Chitosan with bioactive molecules : A sustainable approach for advanced film development. *International Journal of Molecular Sciences, 26*(1–25), Article 10403.

Muñoz-Núñez, C., Hevilla, V., Zágora, J., Plachá, D., Muñoz-Bonilla, A., & Fernández-García, M. (2024). Functionalization of Chitosan-Chitin nanowhiskers films by impregnation with essential oils via supercritical CO2. *Journal of Polymers and the Environment*. https://doi.org/10.1007/s10924-024-03413-3

Muñoz-Nuñez, C., Quiroz-Pereira, Y., Muñoz-Bonilla, A., & Fernández-García, M. (2025). Enhancing antimicrobial and antioxidant properties of chitosan-based films with 1-methylimidazolium-chitosan. *Polymers, 17*(1–26), 2608.

Nwe, N., Furuike, T., & Tamura, H. (2009). The mechanical and biological properties of Chitosan scaffolds for tissue regeneration templates are significantly enhanced by Chitosan from Gongronella butleri. *Materials, 2*(2), 374–398. https://doi.org/10.3390/ma2020374

Paillet, M., & Dufresne, A. (2001). Chitin Whisker reinforced thermoplastic nanocomposites. *Macromolecules, 34*(19), 6527–6530. https://doi.org/10.1021/ma002049v

Patel, D. K., Dutta, S. D., Hexiu, J., Ganguly, K., & Lim, K.-T. (2022). 3D-printable chitosan/silk fibroin/cellulose nanoparticle scaffolds for bone regeneration via M2 macrophage polarization. *Carbohydrate Polymers, 281*, Article 119077. https://doi.org/10.1016/j.carbpol.2021.119077

Peers, S., Montembault, A., & Ladavière, C. (2020). Chitosan hydrogels for sustained drug delivery. *Journal of Controlled Release, 326*, 150–163. https://doi.org/10.1016/j.jconrel.2020.06.012

Petrova, V. A., Golovkin, A. S., Mishanin, A. I., Romanov, D. P., Chernyakov, D. D., Poshina, D. N., & Skorik, Y. A. (2020). Cytocompatibility of Bilayer scaffolds Electrospun from Chitosan/Alginate-Chitin nanowhiskers. *Biomedicines, 8*(9), 305. https://doi.org/10.3390/biomedicines8090305

Pezeshki-Modaress, M., Zandi, M., & Rajabi, S. (2018). Tailoring the gelatin/chitosan electrospun scaffold for application in skin tissue engineering: An in vitro study. *Progress in Biomaterials, 7*(3), 207–218. https://doi.org/10.1007/s40204-018-0094-1

Phongying, S., Aiba, S., & Chirachanchai, S. (2007). Direct chitosan nanoscaffold formation via chitin whiskers. *Polymer, 48*(1), 393–400. https://doi.org/10.1016/j.polymer.2006.10.049

Qasim, S. B., Husain, S., Huang, Y., Pogorielov, M., Deineka, V., Lyndin, M., Rawlinson, A., & Rehman, I. U. (2017). In- vitro and in -vivo degradation studies of freeze gelated porous chitosan composite scaffolds for tissue engineering applications. *Polymer Degradation and Stability, 136*, 31–38. https://doi.org/10.1016/j.polymdegradstab.2016.11.018

Samal, S. K., Dash, M., Chiellini, F., Wang, X., Chiellini, E., Declercq, H. A., & Kaplan, D. L. (2014). Silk/chitosan biohybrid hydrogels and scaffolds via green technology. *RSC Adv., 4*(96), 53547–53556. https://doi.org/10.1039/C4RA10070K

Sauperl, O., Zemljic, L. F., Valh, J. V., & Tompa, J. (2021). Assessment of chemically and enzymatically modified chitosan with eugenol as a coating for viscose functionalization for potential medical use. *Textile Research Journal, 91*(23–24), 2813–2832. https://doi.org/10.1177/00405175211021446

Schmidt, D. R., Waldeck, H., & Kao, W. J. (2009). Protein adsorption to biomaterials. *Biological interactions on materials surfaces* (pp. 1–18). Springer US. https://doi.org/10.1007/978-0-387-98161-1_1

Shagdarova, B., Lunkov, A., Il'ina, A., & Varlamov, V. (2019). Investigation of the properties of N-[(2-hydroxy-3-trimethylammonium) propyl] chloride chitosan derivatives. *International Journal of Biological Macromolecules, 124*, 994–1001. https://doi.org/10.1016/j.ijbiomac.2018.11.209

Sharma, C., Dinda, A. K., Potdar, P. D., Chou, C.-F., & Mishra, N. C. (2016). Fabrication and characterization of novel nano-biocomposite scaffold of chitosan–gelatin–alginate–hydroxyapatite for bone tissue engineering. *Materials Science and Engineering: C, 64*, 416–427. https://doi.org/10.1016/j.msec.2016.03.060

Shen, T., Dai, K., Yu, Y., Wang, J., & Liu, C. (2020). Sulfated chitosan rescues dysfunctional macrophages and accelerates wound healing in diabetic mice. *Acta Biomaterialia, 117*, 192–203. https://doi.org/10.1016/j.actbio.2020.09.035

Sriupayo, J., Supaphol, P., Blackwell, J., & Rujiravanit, R. (2005). Preparation and characterization of α-chitin whisker-reinforced chitosan nanocomposite films with or without heat treatment. *Carbohydrate Polymers, 62*(2), 130–136. https://doi.org/10.1016/j.carbpol.2005.07.013

Tejero, R., López, D., López-Fabal, F., Gómez-Garcés, J. L., & Fernández-García, M. (2015). Antimicrobial polymethacrylates based on quaternized 1,3-thiazole and 1,2,3-triazole side-chain groups. *Polymer Chemistry, 6*(18), 3449–3459. https://doi.org/10.1039/c5py00288e

Terkula Iber, B., Azman Kasan, N., Torsabo, D., & Wese Omuwa, J. (2022). A review of various sources of Chitin and Chitosan in nature. *Journal of Renewable Materials, 10*(4), 1097–1123. https://doi.org/10.32604/jrm.2022.018142

Valencia-Sullca, C., Ben Messaoud, G., Sánchez-González, L., Tehrany, E. A., Vargas, M., Atarés, L., & Chiralt, A. (2024). Chitosan films containing encapsulated eugenol in alginate microspheres. *Food Hydrocolloids, 151*(September 2023), Article 109791. https://doi.org/10.1016/j.foodhyd.2024.109791

van den Broek, L. A. M., Knoop, R. J. I., Kappen, F. H. J., & Boeriu, C. G. (2015). Chitosan films and blends for packaging material. *Carbohydrate Polymers, 116*, 237–242. https://doi.org/10.1016/j.carbpol.2014.07.039

Vasconcelos, D. P., Fonseca, A. C., Costa, M., Amaral, I. F., Barbosa, M. A., Águas, A. P., & Barbosa, J. N. (2013). Macrophage polarization following chitosan implantation. *Biomaterials, 34*(38), 9952–9959. https://doi.org/10.1016/j.biomaterials.2013.09.012

Vo, N. T. N., Huang, L., Lemos, H., Mellor, A. L., & Novakovic, K. (2021). Genipin-crosslinked chitosan hydrogels: Preliminary evaluation of the in vitro biocompatibility and biodegradation. *Journal of Applied Polymer Science, 138*(34). https://doi.org/10.1002/app.50848

Wang, D., Romer, F., Connell, L., Walter, C., Saiz, E., Yue, S., Lee, P. D., McPhail, D. S., Hanna, J. V., & Jones, J. R. (2015). Highly flexible silica/chitosan hybrid scaffolds with oriented pores for tissue regeneration. *Journal of Materials Chemistry B, 3*(38), 7560–7576. https://doi.org/10.1039/C5TB00767D

Wang, H., Qian, J., & Ding, F. (2018). Emerging Chitosan-based films for food packaging applications. *Journal of Agricultural and Food Chemistry, 66*(2), 395–413. https://doi.org/10.1021/acs.jafc.7b04528

Wang, W., Xue, C., & Mao, X. (2020). Chitosan: Structural modification, biological activity and application. *International Journal of Biological Macromolecules, 164*, 4532–4546. https://doi.org/10.1016/j.ijbiomac.2020.09.042

Yang, B., Li, X. Y., Shi, S., Kong, X. Y., Guo, G., Huang, M. J., Luo, F., Wei, Y. Q., Zhao, X., & Qian, Z. Y. (2010). Preparation and characterization of a novel chitosan scaffold. *Carbohydrate Polymers, 80*(3), 860–865. https://doi.org/10.1016/j.carbpol.2009.12.044

Zeng, Z., Yang, Y.-J., Tu, Q., Jian, Y.-Y., Xie, D.-M., Bai, T., Li, S.-S., Liu, Y.-T., Li, C., Wang, C.-X., & Liu, A.-P. (2023). Preparation and characterization of carboxymethyl chitosan/pullulan composite film incorporated with eugenol and its application in the preservation of chilled meat. *Meat Science, 198*, Article 109085. https://doi.org/10.1016/j.meatsci.2022.109085

Zhan, X. (2020). Effect of matrix stiffness and adhesion ligand density on chondrogenic differentiation of mesenchymal stem cells. *Journal of Biomedical Materials Research - Part A, 108*(3), 675–683. https://doi.org/10.1002/jbm.a.36847

Zhao, M.-Y., Yin, Y., Yu, X.-W., Sangani, C. B., Wang, S.-F., Lu, A.-M., Yang, L.-F., Lv, P.-C., Jiang, M.-G., & Zhu, H.-L. (2015). Synthesis, biological evaluation and 3D-QSAR study of novel 4,5-dihydro-1H-pyrazole thiazole derivatives as BRAFV600E inhibitors. *Bioorganic & Medicinal Chemistry, 23*(1), 46–54. https://doi.org/10.1016/j.bmc.2014.11.029

Zhou, B., Drusch, S., & Hogan, S. A. (2022). Food hydrocolloids rheological fingerprinting and tribological assessment of high internal phase emulsions stabilized by whey protein isolate : Effects of protein concentration and pH. *Food Hydrocolloids, 131*(March), Article 107816. https://doi.org/10.1016/j.foodhyd.2022.107816